American Journal of Theoretical and Applied Statistics
2026; 15(1): 1-26
http://www.sciencepublishinggroup.com/j/ajtas
doi: 10.11648/j.ijepe.20261501.11

Novel Vertical Axis Wind Turbine Flow Control: Adaptive Flaps and Trailing-edge Splitter

Jianyu Wang[1], Jian Chen[1,*], Yu Zhang[2], Xinrong Su[3], Chun Li[1], Ying Wang[1]

[1]School of Energy and Power Engineering, University of Shanghai for Science and Technology, Shanghai, China
[2]China Railway Rolling Stock Corporation Limited, Beijing, China
[3]Department of Energy and Power Engineering, Tsinghua University, Beijing, China

Email address:

09900589R@connect.polyu.hk (Jian Chen)
*Corresponding author

To cite this article:

Jianyu Wang, Jian Chen, Yu Zhang, Xinrong Su, Chun Li, Ying Wang. (2026). Novel Vertical Axis Wind Turbine Flow Control: Adaptive Flaps and Trailing-edge Splitter. *American Journal of Theoretical and Applied Statistics, 15*(1), 1-26.
https://doi.org/10.11648/j.ijepe.20261501.11

Received: 25 November 2025; **Accepted:** 15 December 2025; **Published:** 20 January 2026

Abstract: Dynamic stall occurring the operation of vertical axis wind turbine (VAWT) have attracted great attention in the field of wind power due to their detrimental effects on aerodynamic performance. Extensive flow control strategies have been conducted to alleviate the adverse effects of dynamic stall on aerodynamic performance. This study proposed the active control of adaptive flaps and innovatively introduced a trailing-edge splitter plate as a control method to improve the aerodynamic performance of VAWT. A computational fluid dynamics (CFD) simulation is conducted to investigate the influence of two flow control methods on the aerodynamic performance of a National Advisory Committee for Aeronautics (NACA) 0015 airfoil and a VAWT. The findings indicate that the adaptive flap should be positioned at the trailing edge. An optimal deployment angle exists across various angles of attack (AOA), with the flap length of 0.15c determined as most effective for flow separation control at moderate Reynolds numbers. In pre-stall, the splitter plate achieves a maximum lift-drag ratio improvement of approximately 61.6% (l = 0.2c). Regarding the application effects of both flow control methods on the VAWT, the flaps can significantly reduce the vortex size near the blades and promote vortex shedding near the blades. At λ = 1.2-2.0, the flaps can improve the power coefficient factor of the VAWT by up to 42.5% (λ = 1.6).The splitter plate can increase the power coefficient of the VAWT by a maximum of about 29.4% (λ = 0.8) at low TSRs (λ = 0.4 to 1.2). At high TSRs (λ = 2.0 to 2.4), the splitter plate can increase the power coefficient by a maximum of about 25.8% (λ = 2.8).

Keywords: Flow Control Technologies, Active Control Technologies, Aerodynamic Performance, VAWT

1. Introduction

Global warming, the frequency of extreme weather events, and increased energy demand have led to a global shortage of energy supply [1, 2]. Consequently, the energy transition is imperative, and the development of renewable energy is paramount [3]. In recent years, wind energy has experienced rapid growth as a source of renewable energy. Wind turbines are indispensable in the generation of electricity from wind energy [4]. The classification of wind turbines is based on the direction of the axis of rotation, with horizontal axis turbines (HAWT) and vertical axis turbines (VAWT) being the two primary categories [5, 6]. VAWTs have the advantages of low installation cost, low noise [7, 8] and no yawing device [9]. However, the deployment of wind energy by VAWTs remains relatively limited due to its low power coefficient. To improve the power coefficient of VAWTs, extensive scholars have used flow control techniques to enhance the aerodynamic performance of VAWT [10]. Flow control technologies are divided into passive and active flow control technologies based on whether or not an energy input is required [11]. Active flow control requires additional energy input. Qian et al. [12] numerically investigated the aerodynamic performance of the FFA-W3-241 airfoil with deformable trailing edge flaps to reduce unsteady loads under dynamic stall conditions. Carla

Attie et al. [13] optimized the performance of the H-type Darrieus VAWT by employing single-slotted deflector flaps at the trailing edge of the blade. Wang et al. [14] effectively suppressed the formation and development of separation vortices by utilizing boundary layer suction to eliminate the low-momentum fluid at the leading edge of the airfoil suction. Sun et al. [15] utilized blowing and suction flow control to investigate the impact of the rotating flow field of the blade, thereby ascertaining that the net output power could be augmented. Notwithstanding the fact that active control technology has the capacity to increase the complexity of the overall system [16], its strengths are even more pronounced in the aeronautical aviation sector [17]. Conversely, passive flow control methods do not necessitate external energy input and are comparatively more straightforward to implement [18-19]. Passive flow control involves the implementation of shape-altering and add-on structures on the airfoil. In general, shape altering method including recessed cavity and the J-type airfoil. The recessed cavity constitutes a passive method of controlling the flow separation of the airfoil by opening an inwardly recessed cavity on the surface of the airfoil. Sobhanni et al [20] introduced inward-facing pits (cavities) on the NACA0021 airfoil and applied them to a vertical axis wind turbine and found to improve the torque output of the wind turbine. It was also found that the use of dimples in the pressure plane can be effective at all tip speed ratios (TSR), and that the arrangement in the suction plane is only effective at high TSRs. Additionally, dimples were found to induce smaller separation vortices on the blade, which diffuse more rapidly. In their seminal study, Yoo and Oh et al [21] investigated the effect of cavity parameters, including diameter, depth and location of the cavity on vertical axis wind turbines. Specifically, their findings revealed that the location of the cavity has the most significant impact on the wind turbine performance: when the cavity is placed near the trailing edge of the blade, the power coefficient of the wind turbine increases. Although the cavity can occasion delay the flow separation, excessively large or deep cavities can further diminish the stiffness of the wind turbine blades, rendering the wind turbine prone to damage. Therefore, some studies have utilized multiple small dimples instead of a single large cavity to enhance the aerodynamic performance of the airfoil while minimizing the degradation of blade stiffness. The J-type airfoil is controlled by the removal of part of the profile on the pressure measurement or suction side of the airfoil. Zamani et al. [22-24] examined the J-type airfoil and concluded that the J-type airfoil is capable of utilizing both drag and lift. This enhances the torque of the wind turbine at low TSR conditions and improves its self-starting capability. The add-on structures on the airfoil include Gurney flaps, a leading edge slit wing and adaptive flaps. Gurney flaps are used to modify the load distribution of an airfoil by altering the configuration of the trailing edge, thereby facilitating load control of the airfoil. Shukla [25] conducted an investigation into the aerodynamic characteristics of NACA airfoils with pits, Gurney flaps, and both pits and Gurney flaps. The findings indicate that the aerodynamic efficacy of the airfoil equipped with both pits and Gurney flaps surpasses that of the airfoil with Gurney flaps alone when the AOA is less than 12°. A leading-edge slit wing is defined as an aileron (slit wing) that is mounted in close proximity to the leading edge of the main wing, with the purpose of creating a channel through which fluid can flow more rapidly from the pressure side to the suction side of the main wing. Yavuz [26] investigated the hydrodynamics of an airfoil with a leading edge slit wing and the application of a leading edge slit wing to a wind turbine through the numerical simulations and experiments. The findings indicate that the leading edge slit wing has the capacity to delay the stall AOA by 7° and augment the maximum lift coefficient by 191.7%. However, the incorporation of a leading edge slit wing will result in an increase in the complexity of the blade system and the weight of the blade. Adaptive flaps are also classified as a flow control method, which adds structure to an airfoil. Bramesfeld [27] et al. installed self-adaptive flaps on the S824 airfoil and conducted experimental investigations into its flow control effect, which showed that the lift coefficient could be improved by about 20% relative to the original airfoil. Weider [28] et al. investigated the effect of different parameters of adaptive flaps on the NACA0020 airfoil at low Reynolds number, and the results showed that adaptive flaps can reduce the reversed flow area and can prevent the airfoil from stalling. Compare to other flow control methods, the adaptive flap is a passive flow control method with simple structure and better control effect. The installation of flaps on the suction surface of the airfoil enables control to be achieved by altering the parameters of the flaps. Notably, the adaptive flap is essentially different from the aforementioned Gurney flaps: while Gurney flaps are typically mounted at the trailing edge of the airfoil, the adaptive flap is installed on the suction surface, and its adjustable parameters are more flexible in comparison. However, the current researches on flaps are predominantly focused on the passive flaps, and there are fewer studies on active control of adaptive flaps. It is imperative to investigate the impact of adaptive flaps on the aerodynamic performance of thin airfoils at medium and high Reynolds numbers, given the demonstrated capacity of the thin airfoil to enhance the aerodynamic performance of VAWTs [29]. In addition, an extensive literature review reveals that splitter plates mounted behind circular cylinders can effectively reduce the interference of wake flow on the cylinders and mitigate fluctuations in their lift and drag coefficients [30, 31]. Inspired by this well-documented aerodynamic benefit, this paper proposes a novel flow control device-specifically, a splitter tab installed downstream of the airfoil's trailing edge and aims to systematically investigate its effects on the aerodynamic performance of the airfoil. Notably, to the best of our knowledge, the impact of such a splitter tab configuration on airfoil aerodynamic performance remains an unaddressed research gap in current academic investigations. In this paper, the effect of adaptive flaps and trailing edge splitter plate on the aerodynamic performance of NACA0015 airfoil was investigated in different parameters. Then, the active flow control method of adaptive flaps and trailing edge splitter plate are applied to the VAWT, and the aerodynamic performance of the VAWT with the two flow control methods is compared and analyzed.

2. Geometry of Models

In this section, the geometry of airfoil and VAWT are presented. The original airfoil and airfoil with two kinds of flow control methods are described in the firstly place. VAWT and its related parameters are described in the following section.

2.1. Geometry of Airfoil

The NACA0015 airfoil is shown in Figure 1(a), it is a symmetrical airfoil, the chord length (c) of the airfoil which is 0.4m. Figure 1(b) shows the airfoil with flap. Δs is the distance between the flap and the leading edge of the airfoil. lf is the length of flap, and θ is the angle between the flap and the airfoil. Figure 1(c) is an airfoil with a trailing edge splitter plate. The f is the distance between the splitter plate and trailing edge of the airfoil, the length of the plate is l.

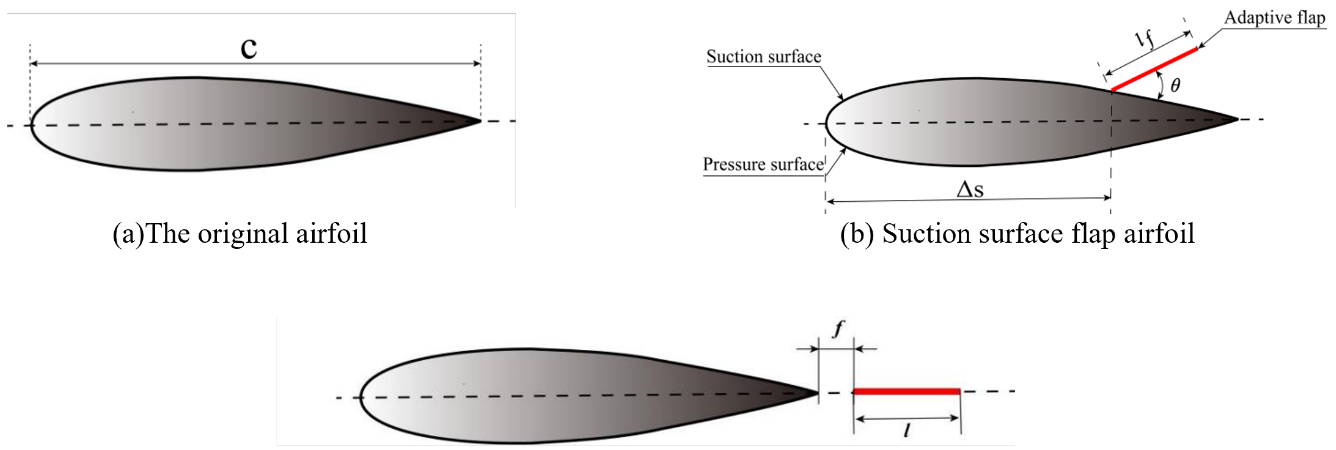

(a)The original airfoil (b) Suction surface flap airfoil

(c) Airfoil with a trailing edge splitter plate

Figure 1. *Three different types of airfoil.*

2.2. Geometry of VAWT

The rated power of the original VAWT is 3kW whose top view is shown in Figure 2.Its design parameters are enumerated Table 1. Figure 2(b) and Figure 2(c) are the views of VAWTs with adaptive flaps and trailing edge splitter plates. D is the diameter of the wind turbine. In order to present the models in a more intuitive manner, 3D models are introduced in Figure 3.

Table 1. *Parameters of VAWT.*

Item	Value
Type of airfoil	NACA0015
Number of blades	3
Shape of blade	H type
Radius of rotation(mm)	1400
Chord length(mm)	420
Solidity	0.45

3. Numerical Calculation Method

3.1. Governing Equation and Turbulence Model

This paper applies the mass conservation equation (1) and momentum conservation equation (2), the equations are expressed as:

$$\frac{\partial \rho}{\partial t}+\frac{\partial(\rho u)}{\partial x}+\frac{\partial(\rho v)}{\partial y}+\frac{\partial(\rho w)}{\partial z}=0 \quad (1)$$

$$\frac{\partial\left(\rho \bar{u}_i\right)}{\partial t}+\frac{\partial\left(\rho \bar{u}_i \bar{u}_j\right)}{\partial t}=-\frac{\partial \bar{p}}{\partial x_i}+\frac{\partial\left\{\mu \frac{\partial u_i}{\partial x_j}-\rho \overline{u_i \dot{u}_j}\right\}}{\partial x_j} \quad (2)$$

The SST $k-\omega$ model has been demonstrated that a high degree of accuracy in the prediction of both the near-wall and mainstream regions. It is widely used in boundary layer flow and separation transition prediction [32]. It is widely used in the field of wind turbine aerodynamic performance prediction and airfoil flow control research [33]. The SST $k-\omega$ model equations are as follows:

$$\rho\left(\frac{\partial \omega}{\partial t}\right)+\frac{\partial \omega u_i}{\partial x_i}=\frac{\partial}{\partial x_j}\left(\Gamma_\omega \frac{\partial \omega}{\partial x_j}\right)+G_\omega-Y_\omega+S_\omega \quad (3)$$

$$\rho\left(\frac{\partial k}{\partial t}+\frac{\partial k u_i}{\partial x_i}\right)=\frac{\partial}{\partial x_j}\left(\Gamma_k \frac{\partial k}{\partial x_j}\right)+G_k-Y_k+D_k \quad (4)$$

In this equation, k and ω represent turbulent kinetic energy and specific dissipation rate, respectively. "Γ", "G", and "Y" denote the turbulent diffusion coefficient, production term, and dissipation term, respectively. D is the additional cross-diffusion term, and S represents a user-defined source term.

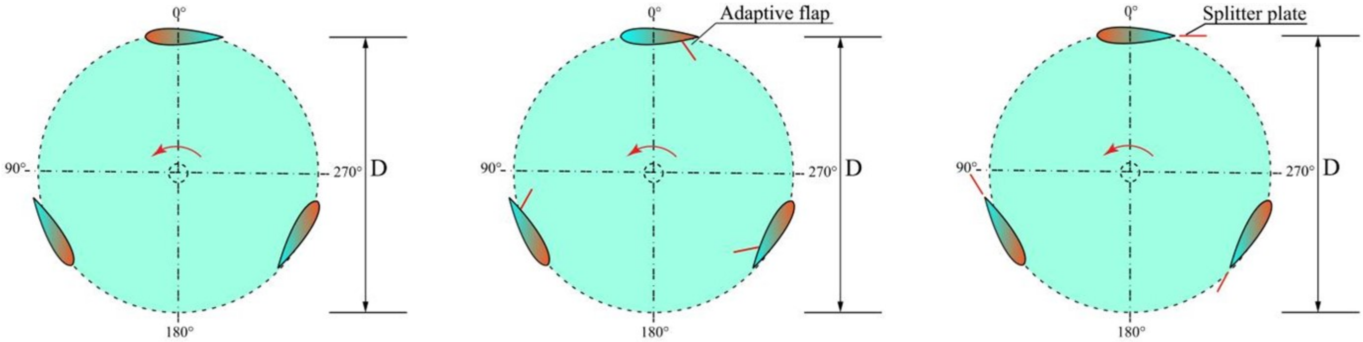

***(a)** VAWT of original.* ***(b)** VAWT-Adaptive flap.* ***(c)** VAWT-Splitter plate.*

***Figure 2.** 2D top views of VAWT with different types of airfoil.*

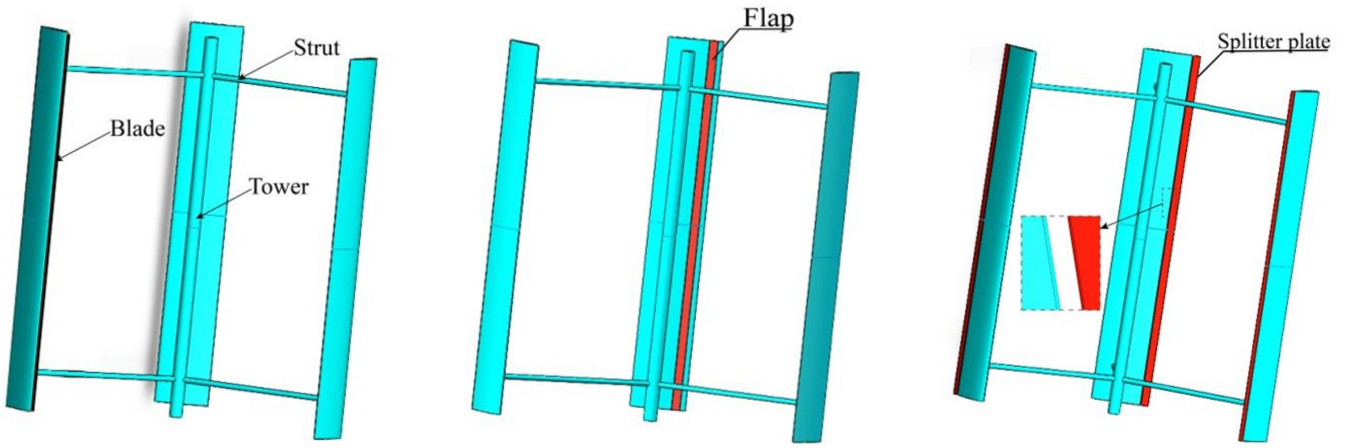

***(a)** Original VAWT.* ***(b)** VAWT with flaps.* ***(c)** VAWT with splitter plates.*

***Figure 3.** 3D views of VAWT with different types of airfoils.*

3.2. CFD Strategies for the Aerodynamic Simulation of Airfoil

3.2.1. Computational Domain and Boundary Condition

As shown in Figure 4, the computation domain of the airfoil is divided into inner and external domains. The data exchange between internal and external domains is carried out through the INTERFACE. Based on literature [5], the inlet boundary is defined as the velocity inlet; the outlet is defined as the pressure outlet, the upper and lower wall surfaces are defined as the symmetric boundary. The airfoils are set as the WALL (no-slip wall surface boundary). The size of the external domain is $14c \times 50c$, the inner domain is a circle with a diameter of 6c, the airfoil is placed at the center of the vertical direction, the distance between the center of the airfoil and the inlet is 12.5c. The outlet boundary is 37.5c away from the aerodynamic center, and the upper and lower wall boundaries are 7c away from the aerodynamic center each. The distance between the two symmetric boundaries is 14c.

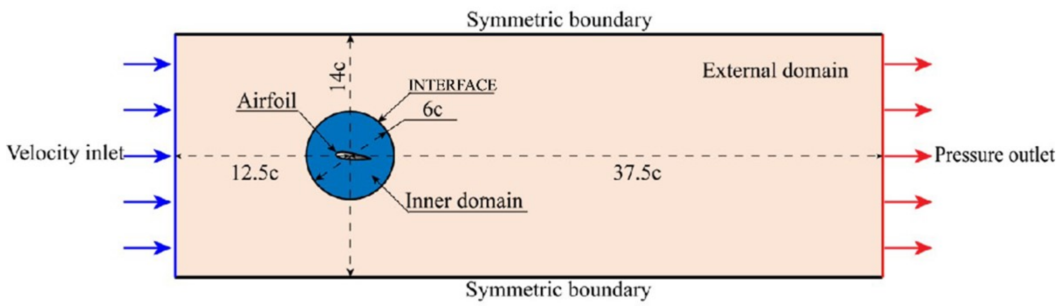

***Figure 4.** Computation domain of airfoil.*

3.2.2. Mesh and Independent Validation of the Mesh

The ICEM CFD is used to discretize the computational domain showed in Fig. The unstructured mesh is used in the inner domain. The 200 nodes are arranged at the interface between the inner and external domains, which ensure the accuracy of the interpolation calculation at interface. The overall mesh size of the external and inner domains is 0.1m and 0.4m respectively, the number of nodes on the airfoil is 800. In order to satisfy the requirements of the SST k-ω turbulence model and to obtain accurate results and flow conditions around the airfoil, the height of the first layer of the boundary layer around the airfoil is4×10^{-5} m, the growth rate of the boundary layer is 1.15. The overall number of the mesh is about 99,800, and the number of the mesh nodes is about 65,000. 5.

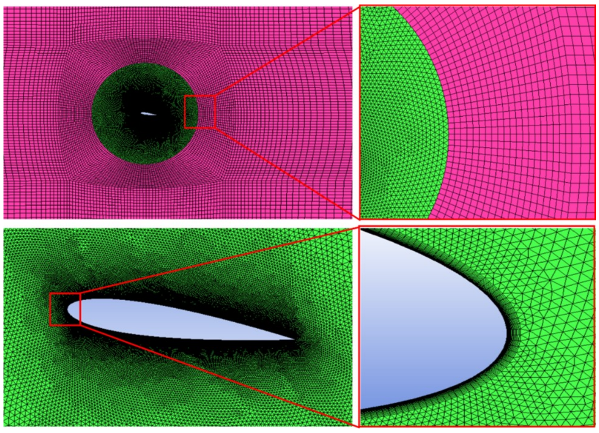

Figure 5. *Mesh of Computation Domain.*

To study the mesh independence, the mesh size of the inner and outer domain is changed to gain different mesh number. Five sets of meshes are selected under the working condition with $Re = 3.6 \times 10^5$ and AOA = $8°$, as shown in Table 2.

Table 2. *Number of meshes for the airfoil.*

Case	Mesh size of inner domain	Mesh size of external domain	Mesh nodes on the airfoil (pcs	Total number of meshes (million)
M1	0.1	0.16	100	5.7
M2	0.08	0.14	400	6.63
M3	0.06	0.12	600	8.17
M4	0.04	0.1	800	9.98
M5	0.02	0.08	1200	10.77

The calculation results are shown in Figure 6, it can be seen that from the cases of M1 to M3, the lift and drag coefficient are greatly affected by the number of meshes. For cases of M4 to M5, the results for the aerodynamic parameters change less with the increase in the number of meshes, so the case of M4 is selected.

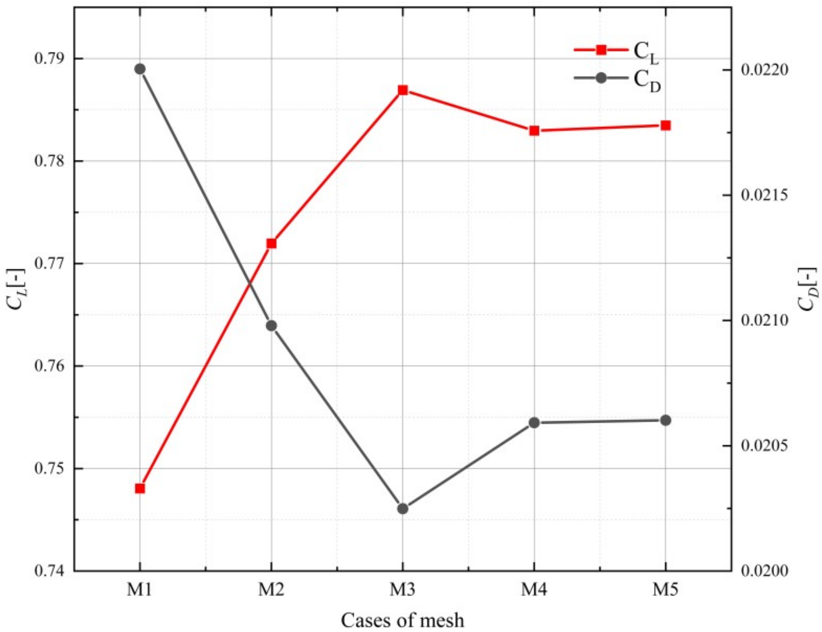

Figure 6. *Variation of lift and drag coefficients with the number of mesh.*

3.2.3. Comparison between CFD Computed Values and Experimental Values

To verify the reliability of the computational model, the aerodynamic parameters of the NACA0015 airfoil were calculated using the ANSYS FLUENT solver at a Reynolds number (Re) of 3.6×10^5 and an angle of attack (AOA) range of 0°–24°. The CFD simulation results were compared with experimental data, and the comparison is presented in Figure 7.

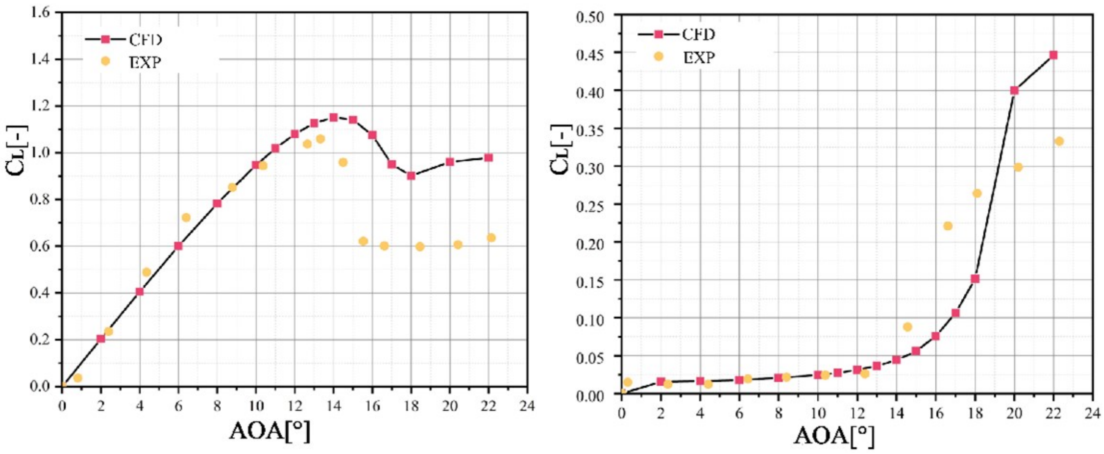

Figure 7. Comparison between CFD Computed Values and Experimental Values.

With the gradual increase in AOA, the simulation results of aerodynamic parameters show good agreement in the variation trend with the experimental data. Particularly in the AOA range of 0°-12°, the CFD results are basically consistent with the experimental data; however, relatively larger errors are observed under large AOA conditions. This is attributed to the stall of the airfoil under large AOA conditions, where the selected turbulence model exhibits reduced solution accuracy for the momentum equation, leading to slight discrepancies from the experimental data. Such discrepancies are unavoidable, but the variation trends remain consistent. Furthermore, this study focuses on the influence of certain flow control methods on the aerodynamic performance of the original airfoil, which is a comparative study of various computational models. Slight deviations in the aerodynamic parameters of the airfoil do not affect the final conclusions. Therefore, the selected computational model is applicable, and the algorithm is reliable.

3.3. CFD Strategies of VAWT

3.3.1. Computational Domain and Boundary Ccondition

A schematic diagram of the VAWT computational domain is shown in Figure 8.

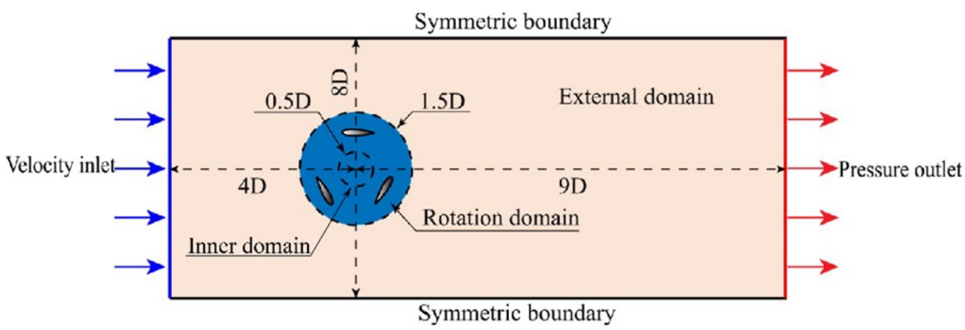

Figure 8. Schematic of the computational domain of VAWT.

The whole computational domain is divided into three parts, which are the external domain, rotational domain and the inner domain including the axis. The rotating domain is a circular area with 1.5D (D is the diameter of the wind turbine) as the large circle and 0.5D as the small circle. The left side of the computational domain is the inlet boundary, the boundary condition is the velocity inlet, the inlet velocity is 13.45 m/s, the distance of the inlet boundary from the center of rotation is 4D; the right side of the computational domain is the pressure outlet boundary, in order to ensure the full development of the wind turbine wake, the outlet boundary is 9D from the center of rotation. the upper and lower boundaries of the computational domain are symmetric boundaries, and the distance from the center of rotation is 4D.

3.3.2. Mesh and Independent Validation of the Mesh

As demonstrated in the Figure 9, the mesh of the computing domain is composed of a structured mesh and an unstructured mesh, with a structured mesh being adopted in the outer domain and the inner domain in proximity to the main axis. As shown in the figure, the mesh around the blades and spindles is locally encrypted due to the complexity of the flow around the blades, flap and plate. The height of the first layer of the mesh on the blade surface is 4×10^{-5}m, which ensures that the requirement of y^+ value less than 1 is met. At the same time, the meshes near the interface of different domains are kept consistent to ensure the accuracy and convergence of the calculation results.

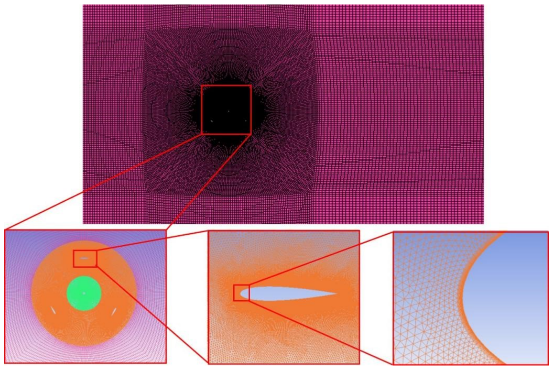

Figure 9. *Schematic of VAWT mesh distribution.*

The validation of mesh independence is achieved through the variation of two parameters: the average mesh size of the rotational domain mesh and the number of mesh nodes on the blade. The validation process involves four sets of meshes. The details of the four cases of Mesh are shown in Table 3.

Table 3. *Number of meshes for VAWT.*

Case	Average mesh size of rotating domain (m)	Number of mesh nodes on the blade	Number of meshes
Mesh1	0.06	400	183138
Mesh2	0.04	800	262232
Mesh3	0.03	1200	387890
Mesh4	0.02	1600	515114

Figure 10 shows the variation curves of instantaneous moment coefficients with azimuth angle for a single blade calculated by different VAWT mesh models for λ = 2.0 and an incoming wind speed of V_∞= 13.45 m/s. It is evident that as the number of grids increases from Mesh1 to Mesh3, the variability of the torque coefficient and azimuth at the peak also increases accordingly. Furthermore, the range of variation in azimuth between 75° and 160° is significantly expanded. The curves for Mesh3 and Mesh4 are consistent with each other, with the only change occurring at the peak. This change does not alter with an increase in the number of grids, indicating grid independence verification. In order to conserve computational resources, the mesh partitioning method of Mesh3 was selected for subsequent studies.

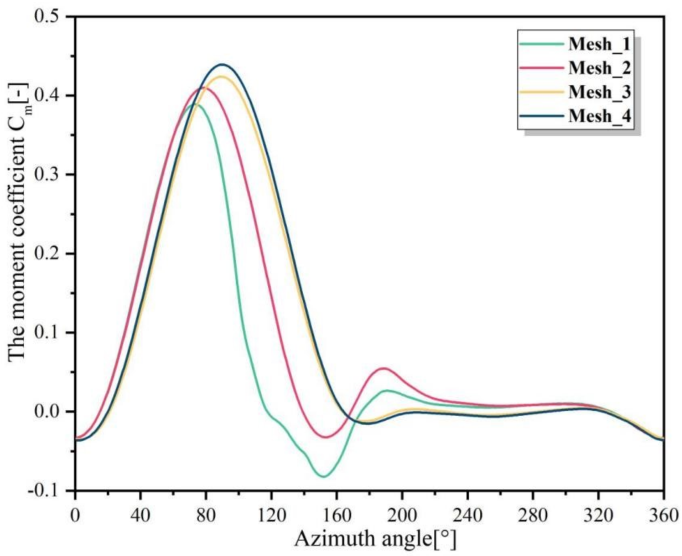

Figure 10. *Variation curve of single blade moment coefficient with azimuth angle for different number of meshes.*

4. Aerodynamic Performances of Airfoil with Suction Surface Flap and Trailing Edge Splitter Plate

4.1. Aerodynamic Performance of Airfoil with Flap on the Suction Surface

In this section, the influence of Δs and θ on airfoil aerodynamic performance are studied. For Δs, flap is evenly distributed on airfoil first to obtain the impact of its general position distribution on the aerodynamic performance of airfoil, and then the best parameter is further refined to obtain more accurate data. For θ, it is evenly divided on a range of 0-90 degrees to investigate the effect of flap on the aerodynamic performance of airfoil at each θ. In this study, the Re = 3.6×10^5, the range of AOA is 4-22 degrees.

4.1.1. Effect of Distance Between the Flap and the Leading Edge

The objective of this subsection is to investigate the fluence of Δs on aerodynamic of airfoil. The flap position of 0.25c, 0.5c and 0.75c are investigated in the first place when the flap angle is 30 degrees and the flap length is 0.15c, as shown in Figure 11(a). The lift and drag coefficients of original airfoil and airfoil with flap are calculated in the range of 4-22 degrees of AOA, as shown in Figure 12.

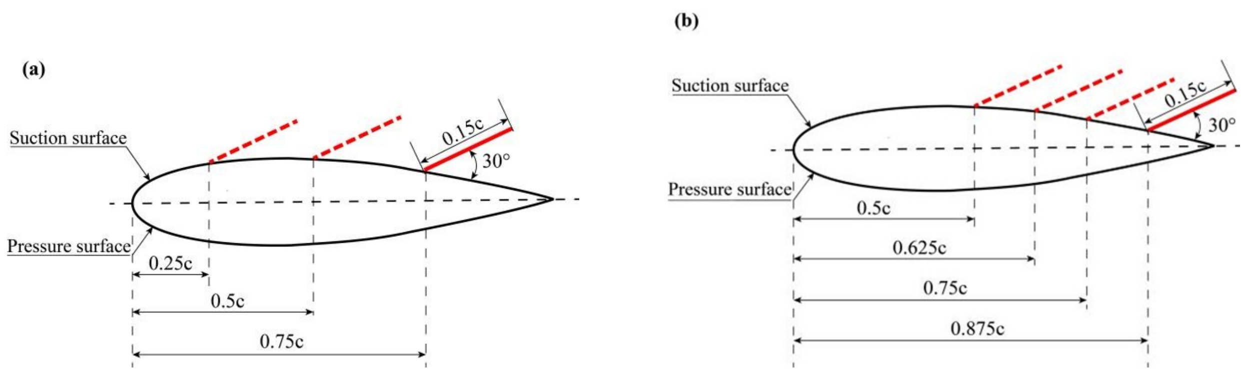

Figure 11. Calculation model for different positions of flaps.

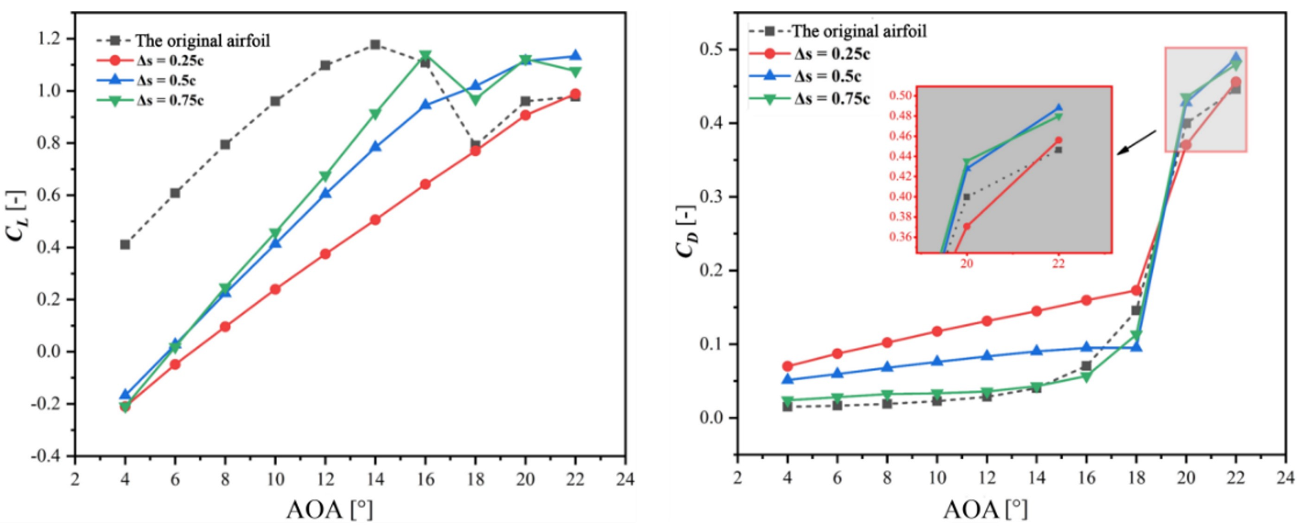

(a) Lift Coefficient (b) Drag coefficient

Figure 12. Lift and drag coefficient variation curves with AOA with different positions of suction surface flaps.

For the lift coefficient, it is found that the flap has a negative effect at the low AOA of airfoil, the closer flap is to the leading edge of the airfoil, the more negative effect is. When the AOA is greater than 16, the flap will play a positive role. It is also worth noting that when Δs = 0.25c, the lift coefficient of the airfoils is lower than the original airfoil at any AOA. For the drag coefficient, when the distance between the flap and trailing edge is small, the drag coefficient will have a small impact. When Δs = 0.25c, the drag of the airfoil is higher than the original airfoil. The lift-drag ratios (LDR) of the airfoil with flap and original airfoil are shown in Figure 13. At low AOA (4°-16°), the LDR of the airfoil with flap is lower than the original airfoil because the flap may destroy the original attachment flow. Furthermore, it has been demonstrated that the rate of change in the LDR is directly proportional to the proximity of the flap position to the trailing edge. At Δs = 0.75c, the LDR of the airfoil with a flap exceeds that of the original airfoil when the AOA is greater than 16 degrees. Similarly, at Δs = 0.5c, the LDR of the airfoil with a flap is superior when AOA exceeds 18 degrees, and at Δs = 0.25c, the airfoil with a flap outperforms the original airfoil when AOA is greater than 20 degrees. This suggests that positioning the flap closer to the trailing edge of the airfoil minimizes adverse effects, allowing the flap to contribute positively at smaller AOA. In summary, no matter where the flap is placed, it will have an adverse effect on the aerodynamic performance of airfoil when the range of AOA is 4-16 degrees. However, it has been demonstrated that the adverse effect is reduced in proportion to the proximity of the position to the trailing edge of the airfoil.

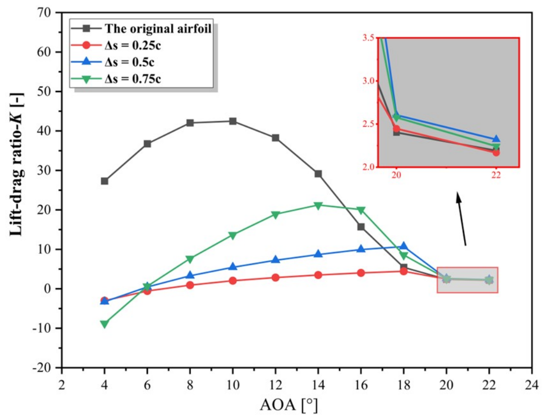

Figure 13. *The LDR of airfoil at different positions of suction surface flaps with different AOA.*

In light of the aforementioned observations, the flap position of 0.5c, 0.625c, 0.75c and 0.875c is the subject of detailed study, as illustrated in Figure 11(b). The variation of lift and drag coefficients of four different flap models and the original airfoil at different AOA is shown in Figure 14. For the lift coefficient, the increase rate of lift coefficient is also different for different Δs as the increase of the AOA. It can be seen that the closer the flap position is to the trailing edge, the less adverse effect is on the airfoil at low AOA. At high AOA($\alpha = 16°$~$22°$), the lift coefficient of the airfoil with flap is higher than the original airfoil. It's worth noting that the lift coefficient of the airfoil with flap is lower than the original airfoil when Δs = 0.875c and α = 20°~22°.

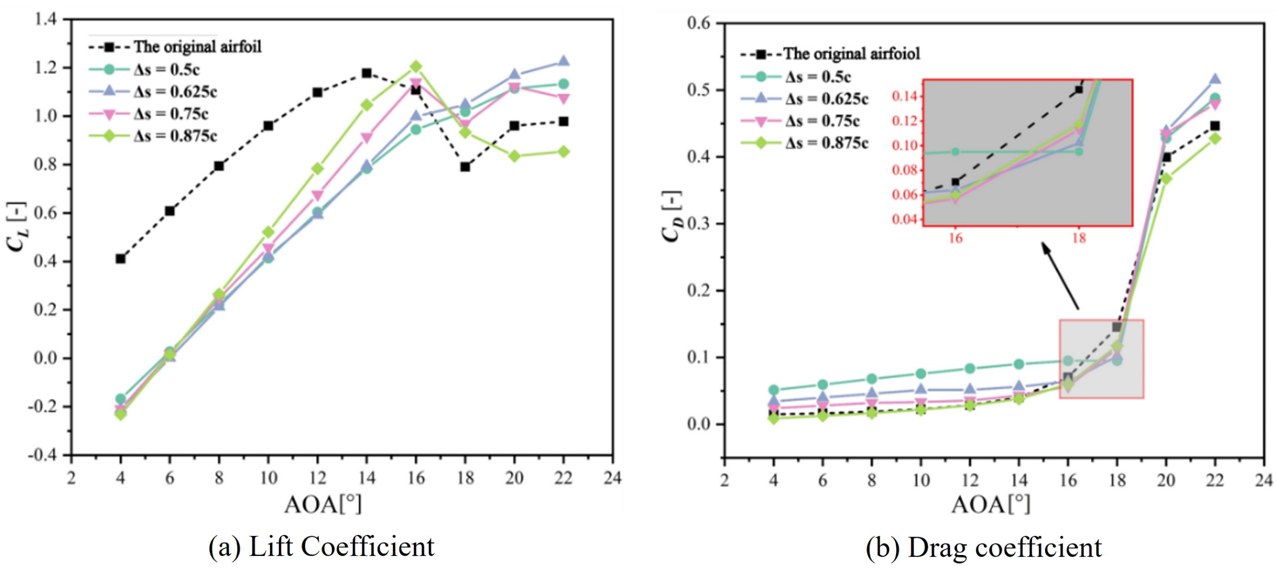

Figure 14. *The variation of lift and drag coefficients of different models with AOA.*

Figure 14(b) shows the drag coefficient. At low AOA, the position is closer to the trailing edge, the less influence is on the drag. At high AOA(α = 16° 22°), the drag of the airfoil with flap is first less than the original airfoil and then greater than the original airfoil, only when Δs=0.875c, the drag of the airfoil is completely smaller than that of the original airfoil. Therefore, the closer the airfoil is to the trailing edge, the smaller the drag is.

In order to study the influence of the position of flap on airfoil aerodynamic performance in total, the variation of LDR of airfoil with AOA under different position of flap is analyzed. As shown in Figure 15,

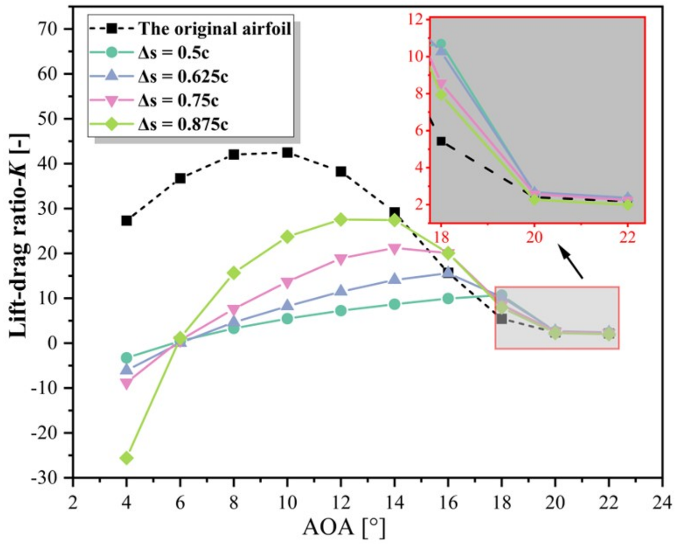

Figure 15. *The variation of lift and drag ratio of different models with AOA*

it can be seen that at a low AOA the closer the position of flap is to the trailing edge, the worse the LDR is. However, an increase in the AOA has been demonstrated to result in a faster rise in the LDR. This is mainly caused by the influence on the lift coefficient of airfoil, and the closer flap is to the trailing edge, the smaller the AOA where the flap plays a positive role. But at a large AOA (α = 20°~22°), the LDR of the model when Δs = 0.875c is lower than the original airfoil. Therefore, the flap should be positioned near the trailing edge. However, it is important to note that positioning it too close to the trailing edge may not necessarily yield better performance.

4.1.2. Effect of the Angle Between the Flap and the Airfoil

The influence of flap angle on aerodynamic performance is studied in this subsection. As shown in Figure 16, the flap position is located 0.75c from the leading edge and the flap length is 0.15c. Five flap angle θ of 30°, 45°, 60°, 75° and 90° are selected for research.

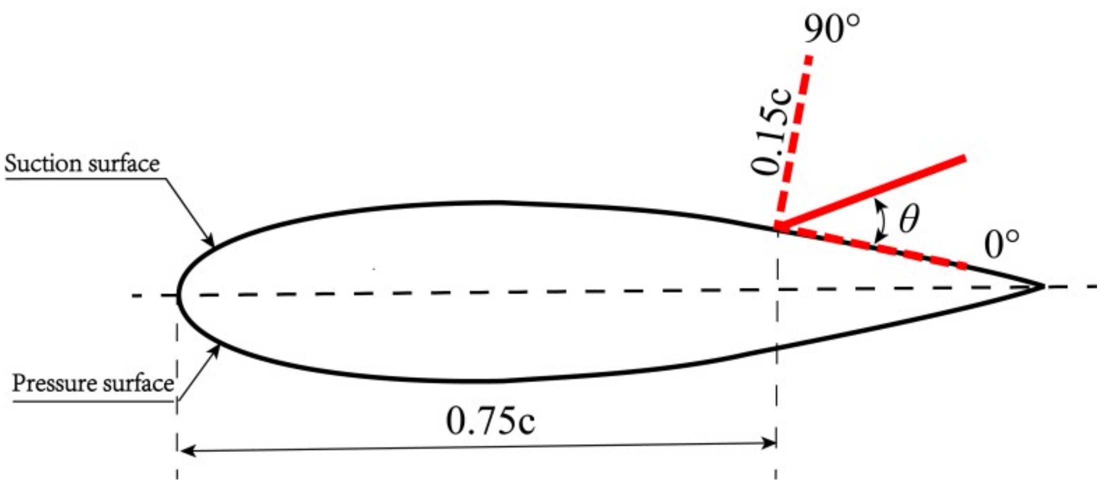

Figure 16. *Schematic diagram of the computational model for different deployment angles of the flaps.*

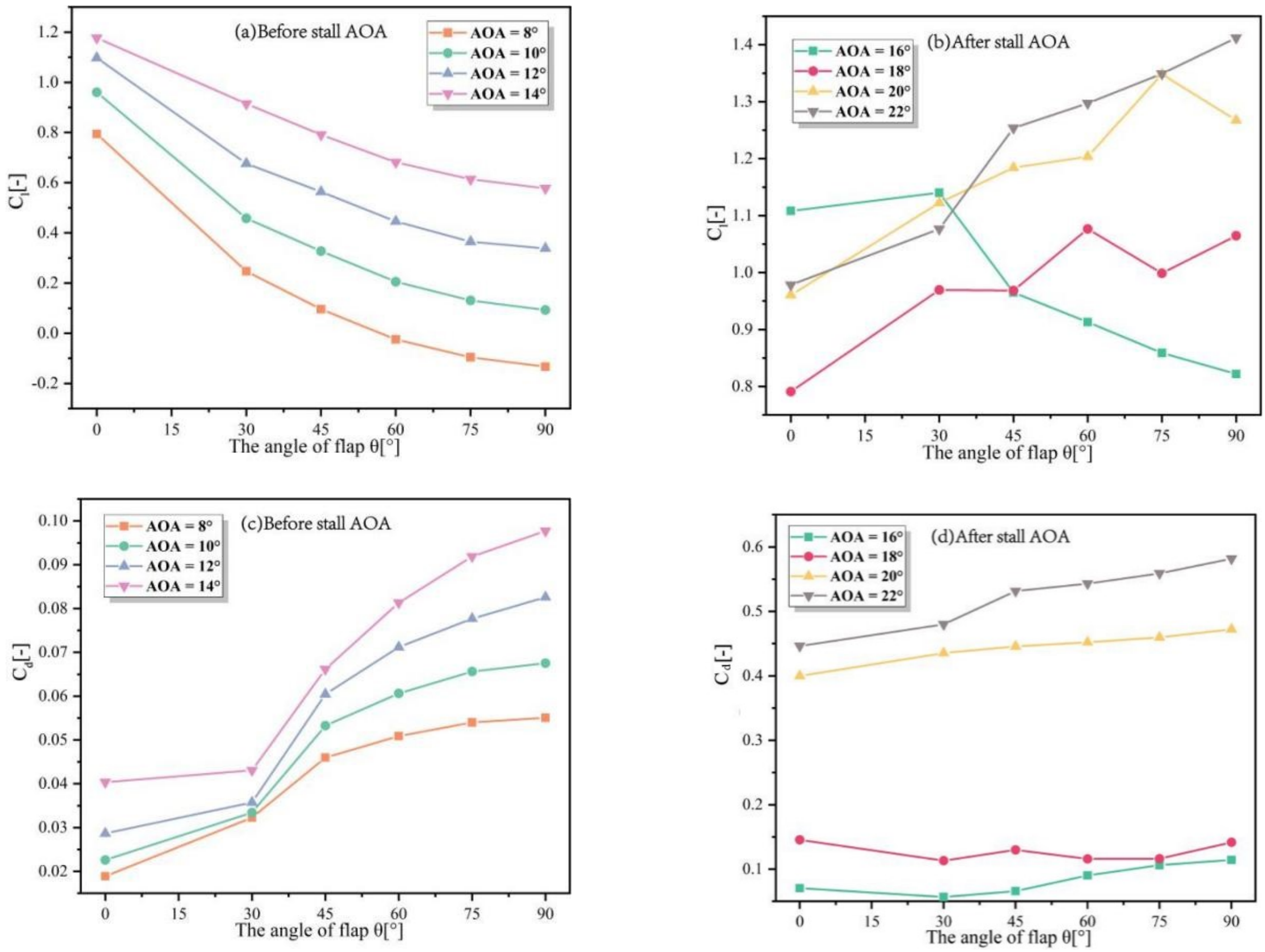

Figure 17. *The variation curve of lift and drag coefficient with flap angle in different AOA*

Figure 17 shows the variation of lift-drag coefficient of airfoil with the flap angle before and after stall angle (about 14°) respectively. In Figure 17(a) and (c), it can be seen that before stall AOA, no matter how much the flap angle is, the flap always has the negative effect, resulting in the lift coefficient decreases and the drag coefficient increases with an increase of θ. In Figure 17(b) and (d), it can be observed that after the stall AOA, the flap angle starts to have the desired effect. When the AOA is 16° and the flap angle exceeds 45°, the lift coefficient of the airfoil with the flap is greater than that of the original airfoil. At AOA values of 18°, 20°, and 22°, the lift coefficient of the airfoil with the flap consistently remains higher than that of the original airfoil. Regarding the drag coefficient, at AOAs of 16° and 18°, the drag coefficient initially increases and then decreases as the flap angle increases. Conversely, at AOAs of 20° and 22°, the drag coefficient rises with an increase in flap angle.

After stall AOA, the flap not only can increase the lift coefficient but also increase the drag coefficient, in order to research the optimum flap angle, the LDR are studied in this section. As can be seen in Figure 18, there is an optimum flap angle at a certain AOA, the optimum flap angles θ = 30°, 60°, 75° and 90° respectively at the AOA of 16°, 18°, 20° and 22°. The optimum flap angle increases with the increase of AOA, but it does not show a linear relationship. The optimal flap angle increases with increasing AOA, but not linearly. Therefore, it may be necessary to adjust the flap angle dynamically.

This dynamic adjustment requirement aligns with Brücker and Weidner [28], who emphasized that “self-adaptive flaps need parameter tuning to suppress stall” for the NACA0020 airfoil, but their study was restricted to low Reynolds numbers ($Re < 1 \times 10^4$). The present study, conducted at moderate Reynolds number ($Re = 3.6 \times 10^5$), demonstrates that dynamic flap angle adjustment can still reduce reversed flow area by $\sim 35\%$ (Figure 18), outperforming the passive flow control using a microcylinder [26] which only achieved stall delay without adaptive optimization.

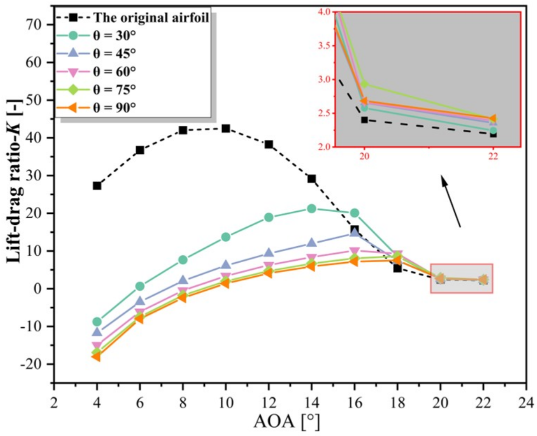

Figure 18. *The variation curve of lift-drag radio with flap angle in different AOA.*

In order to study the influence of the position of flap on airfoil aerodynamic performance in total, the variation of LDR of airfoil with AOA under different position of flap is analyzed. As shown in Figure 15, it can be seen that at a low AOA the closer the position of flap is to the trailing edge, the worse the LDR is. However, an increase in the AOA has been demonstrated to result in a faster rise in the LDR. This is mainly caused by the influence on the lift coefficient of airfoil, and the closer flap is to the trailing edge, the smaller the AOA where the flap plays a positive role. But at a large AOA (α = 20°~22°), the LDR of the model when Δs = 0.875c is lower than the original airfoil. Therefore, the flap should be positioned near the trailing edge. However, it is important to note that positioning it too close to the trailing edge may not necessarily yield better performance.

4.2. Aerodynamic Performance of Airfoil with a Trailing Edge Splitter Plate

4.2.1. Effect of Lengths of Splitter Plate

In this subsection, the influence of different “l” on airfoil aerodynamic performance is studied. As shown in Figure 19, the “l” of 0.05c, 0.1c, 0.15c and 0.2c are selected when the “f” is 0.01c.

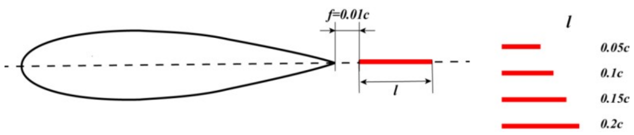

Figure 19. *models for different lengths of splitter plate.*

Figure 20 shows the lift and drag coefficients of the airfoil with different “l” vary with the AOA. For lift coefficient, it can be seen that in the AOA range of 4°-14°, the lift coefficient of the airfoil with splitter plate (AWSP) is higher than the original airfoil. With the increase of the length of splitter plate, the lift coefficient increases. When AOA is 14°, the lift of the AWSP is approximately 21.6% higher than that of the original airfoil (l = 0.2c). When the range of AOA is 14°-16°, the lift coefficient of the AWSP decreases and lower than the original airfoil. When AOA range from 16° to 22°, the lift of AWSP is higher than the original airfoil, the maximum percentage increase is 25.4% (l = 0.2c, α =22°). In general, the splitter plate is helpful in increasing the lift of the airfoil, and with the increase of the “l”, the improvement effect is better.

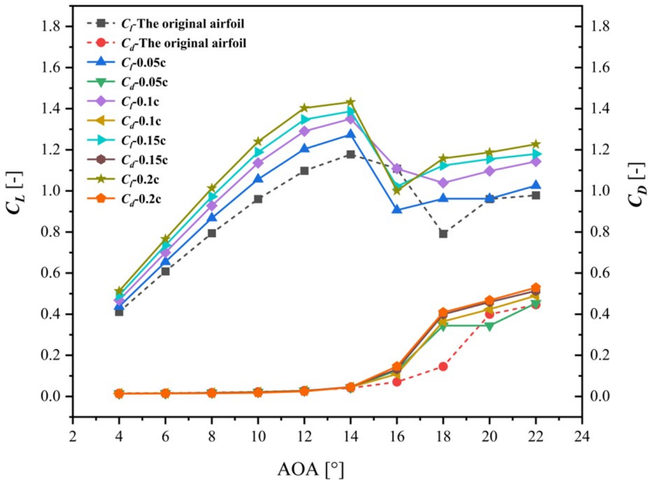

Figure 20. *The lift and drag coefficients of the airfoil with different “l” vary with the AOA.*

The drag coefficients of original airfoil and airfoils with splitter plate remain basically unchanged in the range of small AOA (about 4°-14°), and the drag of the AWSP are lower than the original airfoil. When the range of AOA is 14°-18°, the drag of AWSP is higher than the original airfoil. When the range of AOA is 18°-20°, the drag of the original airfoil is higher. As the AOA increase to the range from 20° to 22°, there is a little difference in drag between the original airfoil and AWSP. The splitter plate will cause adverse effect when AOA is 16°-18°, but the impact is small in general. Therefore, the splitter plate can increase lift and reduce drag at a small AOA.

In order to gain the influence of “l” on the aerodynamic of the airfoil, the LDR is studied in this section. In Figure 21, it can be seen that when the rang of AOA is 4°-14°, the LDR of the AWSP and original airfoil increase firstly and then decrease, and the LDR of the AWSP are higher than the original airfoil, the optimum LDR is achieved when the AOA is 10°, the value of the increase is approximately 61.6% (l = 0.2c). When the range of AOA is 14°-20°, the lift-drag radio of the AWSP is lower than the original airfoil. When the AOA is higher than 20°, the LDR of the AWSP is higher than the original airfoil. Although the splitter plate has a negative effect when the AOA ranges from 14° to 20°, the splitter plate plays a positive role in the aerodynamic performance of the airfoil.

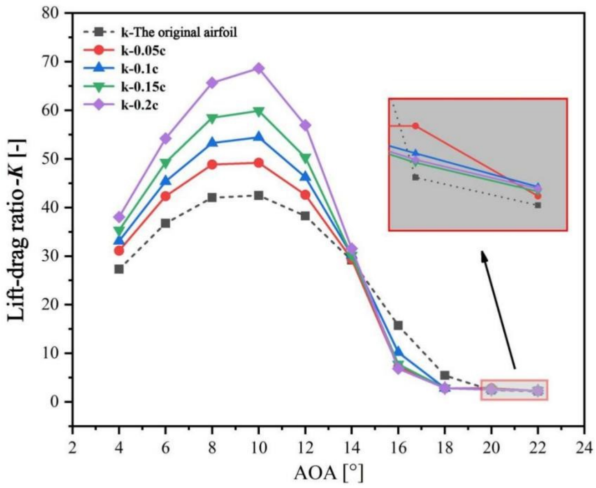

Figure 21. *The LDR of the original airfoil and the airfoil with different lengths of splitter plate varies with the AOA.*

4.2.2. Effect of the Distance Between the Splitter Plate and Trailing Edge

In this subsection, the distance between the splitter plate and trailing edge was investigated. As shown in Figure 22, the "f" of $0.01c$, $0.03c$ and $0.05c$ are selected when the "l" is $0.1c$, the $Re = 3.6 \times 10^5$ and the range of AOA is 4–22 degrees.

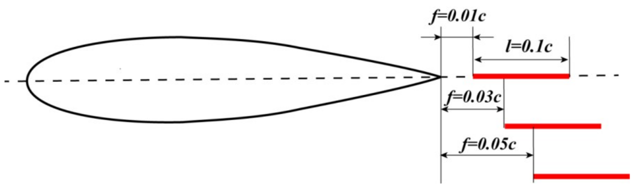

Figure 22. *Schematic diagram of different clearance calculation models.*

Figure 23 shows the lift and drag coefficients of the original airfoil and the airfoil with different "f" of splitter plate varies with the AOA. For lift coefficient, it can be seen that at low AOA (AOA = 4°-14°), the lift coefficient of the AWSP is higher than the original airfoil. But with the increase of the "f", the lift effect of the AWSP decreases, the change is not obvious. Therefore, the change of "f" has little effect on airfoil lift at low AOA. When the range of AOA is 14°-18°, the lift of the airfoil decreases. It is worth noting that when "f" is 0.05c, the lift of the AWSP is 15.2% lower than the original airfoil. When AOA is greater than 18°, the lift of the AWSP is higher than the original airfoil. And as the "f" is reduced, the lifting effect is better, maximum lift increase about 16.8% ("f" = 0.01c). For drag coefficient, the influence of "f" on the drag coefficient is small. When the range of AOA is 4°-14°, the drag coefficient of the AWSP and the original airfoil is no significant difference. When the range of AOA is 16°-18°, the drag coefficient of the airfoil is higher than the original, especially when "f" is small. When AOA is greater than 18°, the influence of "f" on the drag is negligible.

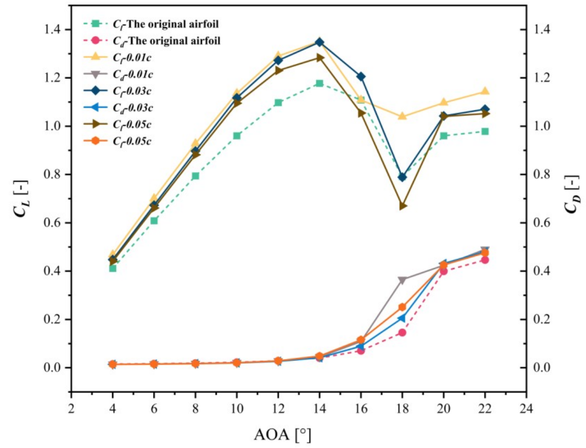

Figure 23. *The lift and drag coefficients of the original airfoil and the airfoil with different "f" of splitter plate varies with the AOA.*

It can be concluded that the distance between the splitter plate and the trailing edge exerts minimal influence on the lift and drag of the airfoil at low AOA. However, when the range of AOA is 16°-18°, it can be seen that "f" exerts a significant influence on the lift and drag of the airfoil. When the AOA exceeds 18°, the parameter "f" exerts a significant influence on lift, while its effect on drag is minimal.

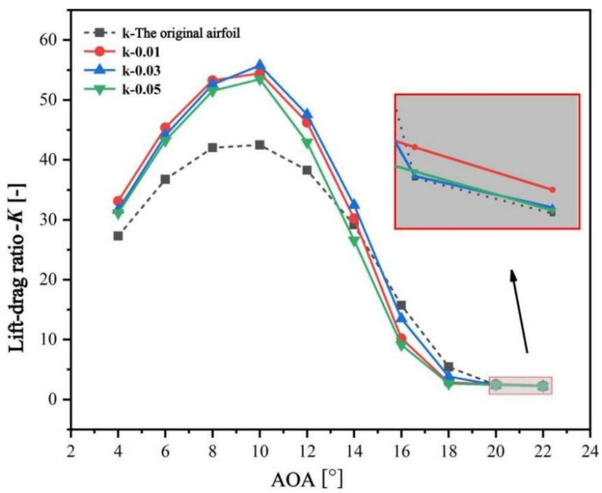

Figure 24. *The LDR of the original airfoil and the splitter plate on airfoil with different "f" varies in different AOA.*

As demonstrated in Figure 24, when the range of AOA is 4°-12°, the LDR of the AWSP is higher than the original. But when AOA is 14°, the LDR of the AWSP is higher than the original when "f" = 0.01c and 0.03c, when "f" = 0.05c, the LDR of the AWSP is lower than the original airfoil. When the AOA ranges from 16°-20°, all the LDRs of the AWSP are lower than the original, but when "f" = 0.03c, the LDR is the best in the AWSP. When the AOA is higher than 20°, the LDR of the AWSP is higher than the original. And the smaller the "f", the better the lifting effect. Therefore, the effect of "f" on airfoil LDR is different for different AOA. Splitter plate will play a positive role at a small AOA (4°-14°), but the influence between different "f" is not significant. When the range of

AOA is 14°-16°, the negative effect on airfoil aerodynamic performance is minimal when "f" = 0.03c. At large AOA (AOA is higher than 20°), the splitter plate has the best effect on the aerodynamic performance of airfoil when "f" = 0.01c.

4.3. Comparison of the Airfoil with Flap and Splitter Plate

Based on the above study, the lift and drag coefficients and LDR of airfoils with flaps and splitter plate at different AOA are compared and analyzed in this section. As demonstrated above, the optimal aerodynamic performance of the airfoil is achieved when the flap length is set at 0.15c, Δs = 0.75c and θ = 30°. This configuration is then compared with the AWSP, as outlined in the subsequent section. In accordance with the aforementioned selection criteria, the length of the splitter plate is determined to be 0.2c, with f being set at 0.01c.

4.3.1. Comparison of Lift and Drag Coefficients

Figure 25 shows the curves of lift and drag coefficient varied with the AOA for different airfoils. For lift coefficient, before stall AOA (about 16°), the CL of the original airfoil is higher than the airfoil with flap and lower than the AWSP. However, after the stall, the CL of the airfoil with flap and splitter plate are both higher than the original airfoil. For drag coefficient, when AOA is less than 14°, original airfoil and AWSP are about the same, the airfoil with flap is slightly higher. When AOA is higher than 14°, the AWSP is higher than the other two. The airfoil with flap is lower than the original airfoil at the range of AOA is 16°-18° and higher than original airfoil at the range of AOA is 20°-22°.

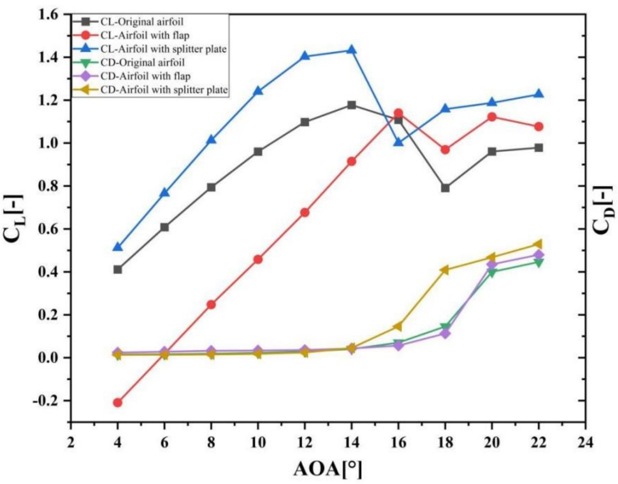

Figure 25. Variation curves of lift and drag coefficient with AOA for different airfoils.

4.3.2. Comparison of LDR

Figure 26 presents the curves of LDR varied with AOA for three airfoils. It is evident shows that the airfoil with flap has a higher LDR than the original airfoil when AOA is greater than 16°, and less than the original airfoil when AOA is less than 16°. The LDR of the AWSP is higher than that of the original airfoil before AOA of 14° and lower than the original airfoil after AOA is 14°, this lends further support to the conclusion that the flap will exert a beneficial effect following a stall, and that the splitter plate will have a favorable effect before a stall occurs.

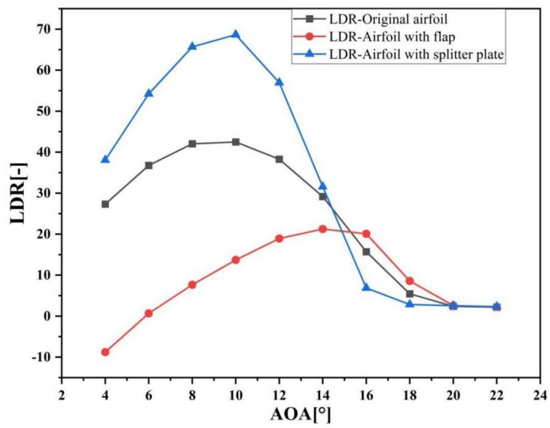

Figure 26. Variation curves of LDR with AOA for different airfoils.

5. Application of Two Flow Control Methods in VAWT

In this section, two flow control methods are applied to the VAWT to investigate their effects on the aerodynamic performance of the VAWT.

5.1. Application of the flap in VAWT

5.1.1. Effect of Flap on VAWT Aerodynamic Performance

The angle of attack of the airfoil during VAWT operation is constantly changing with azimuth. Therefore, the flap may need to be adjusted at different AOA to achieve optimal aerodynamic as mentioned in 3.1.2. It has been concluded that the flap on the airfoil will exert a detrimental effect on aerodynamic performance at low AOA. It follows that the angle of the flap on the airfoil must also be subject to constant modification in order to mitigate the adverse effect at low AOA.

The flap motion control strategy requires the UDF function in Fluent to define the motion of the flaps, which is realized in combination with overlapping grid technology, two control strategies are developed. The first strategy involves a small angle of deployment and high speed, controlled by Equation 5. In this strategy,$\beta_{max1}$is the maximum development angle of flap, which is 30°,$k_{op1}$is the speed of flap movement. This formula shows the control strategy for one turn only.

$$\beta_{op1}(\theta) = \begin{cases} 0°, & 0° < \theta \leq 90° \\ k_{op}(\theta - 90°), & 90° < \theta \leq 130° \\ \beta_{\max1}, & 130° < \theta \leq 140° \\ \beta_{\max1} - k_{op1}(\theta - 140°), & 140° < \theta \leq 180° \\ 0°, & 180° < \theta \leq 360° \end{cases} \tag{5}$$

The second strategy is based on the first strategy, increases the angle of deployment and reduces the speed, which is controlled by Equation 6. $\beta_{\max 2}$ is the maximum development angle of flap, which is 45°, and $k_{\beta 2}$ is the speed of flap movement, where $k_{\beta 2} = \beta_{\max 2}/40°$.

$$\beta_{\beta 2}(\theta) = \begin{cases} 0°, & 0° < \theta \leq 80° \\ k_{op2}(\theta - 80°), & 80° < \theta \leq 120° \\ \beta_{\max 2}, & 120° < \theta \leq 140° \\ \beta_{\max 2} - k_{\beta 2}(\theta - 140°), & 140° < \theta \leq 180° \\ 0°, & 180° < \theta \leq 360° \end{cases} \tag{6}$$

The moment coefficient of the original wind turbine and the wind turbine with two strategies that vary with azimuth angle are presented in Figure 27.

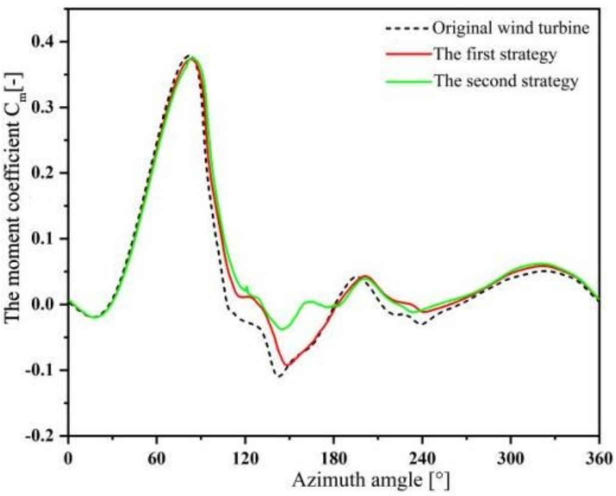

(a) Single blade moment coefficient

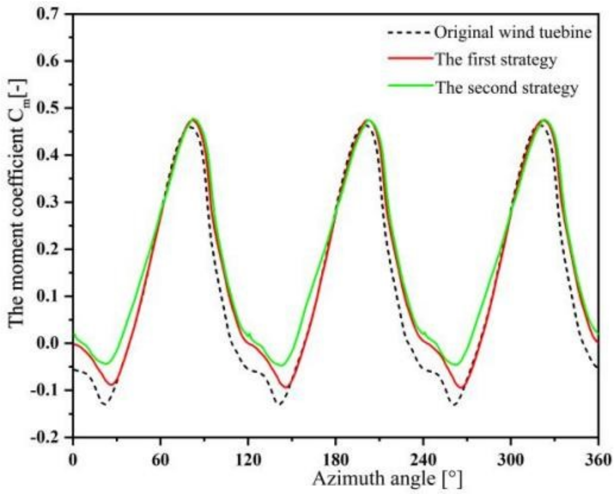

(b) Whole wind turbine moment coefficient

Figure 27. *Change curve of moment coefficient of original wind turbine and wind turbine with two control strategies*

Figure 27(a) is the single blade moment coefficient curve, it can be seen that when the range of azimuth angle is 0°-85°, the three curves of moment coefficient are essentially the same. When the range of the azimuth angle is 85°-180°, the curves of the wind turbine with two control strategies are higher than the original wind turbine, and the second control strategy's moment coefficient curve is higher than the first. The moment coefficient of the whole wind turbine is shown in Figure 27(b), it can be seen that the moment coefficient curves of the wind turbine with the two strategies are also higher than the curve of original wind turbine, and the curve of the second strategy is flatter from the lowest to the highest point, so the second control strategy is better than the first one, and the second control strategy is selected below.

Figure 28 shows the variation curve of moment coefficient of original wind turbine with azimuth angle at different TSR, it can be seen that the azimuth angle of the single blade moment coefficient reaching the peak value is different with different TSR. The smaller the TSR, the easier the wind turbine will stall and the smaller the azimuth angle of stall will be.

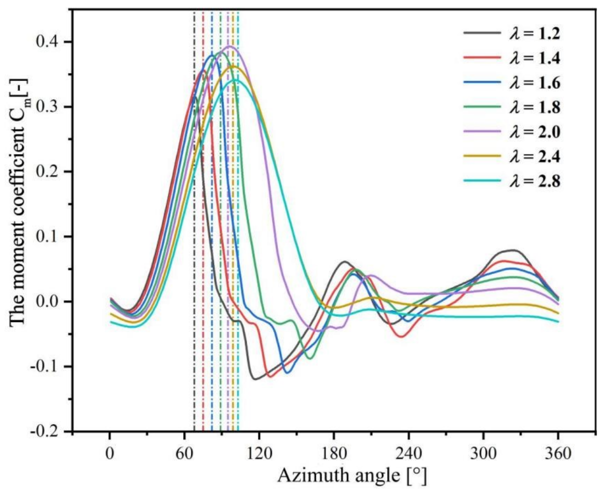

Figure 28. *Change curve of moment coefficient of original wind turbine with azimuth angle in different tip-speed ratio.*

Therefore, a slight change in control strategy is required. The angle of maximum expansion of the flap and the speed of maximum expansion are the same as the second optimized control strategy. The flap begins to expand after the single blade moment coefficient reaches the peak, and the flap is completely closed when the azimuth is 180°.

Figure 29 shows the comparison of power coefficient (CP) before and after flap control method, the λ = 1.2-2.4 and = 13.45 m/s. It can be seen that when the range of the λ is 1.2-2.4, the flap has the best effect on improving aerodynamic performance, maximum increase of power coefficient by 42.5% (when λ = 1.6). When the λ is greater than 2.4, the flap has the adverse effect. The flap would reduce the power coefficient by about 4.4% just as λ = 2.8.

At λ = 1.2 2.0, the flaps can improve the power coefficient factor of the VAWT by up to 42.5% (λ = 1.6). When the λ is greater than 2.4, the flap has the adverse effect. The flap would reduce the power coefficient by about 4.4% just as λ = 2.8. This performance characteristic of the adaptive flap complements the findings of existing studies on passive flow control for VAWTs. Sobhani et al. [20] and Yoo & Oh et al. [21] reported that dimple-modified VAWTs achieve effective power coefficient improvement, primarily in high TSR ranges for suction-side dimples. Zamani et al. [22-24] demonstrated that J-shaped airfoil VAWTs excel in torque enhancement at low TSRs (λ¡1.0) and self-starting capability. In contrast, the present adaptive flap focuses on the medium TSR range (λ=1.2-2.0), where it delivers significant power gains, contributing to the optimization of VAWT performance across a broader operating spectrum. Additionally, the suction-surface mounting design of the adaptive flap maintains blade structural integrity, which aligns with the structural considerations highlighted in Sobhani et al. [20] regarding dimple-induced stiffness concerns.

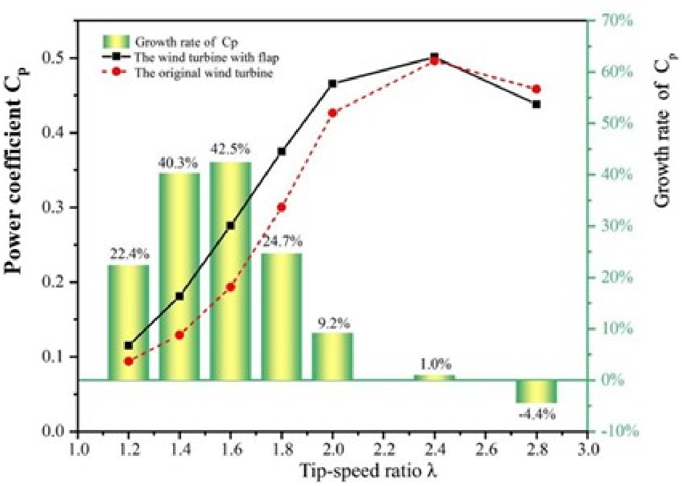

__Figure 29.__ Comparison of power coefficient before and after flap control method.

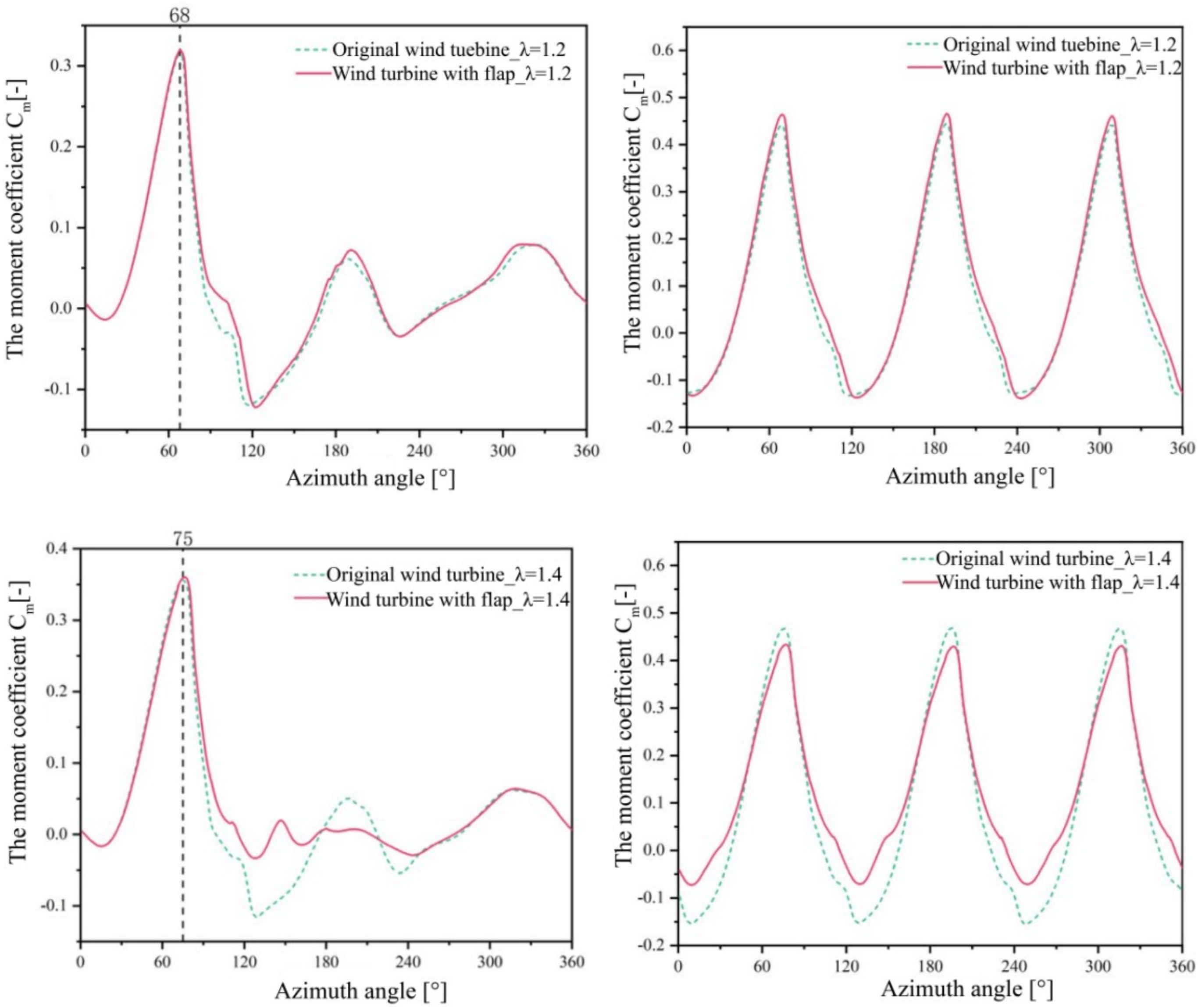

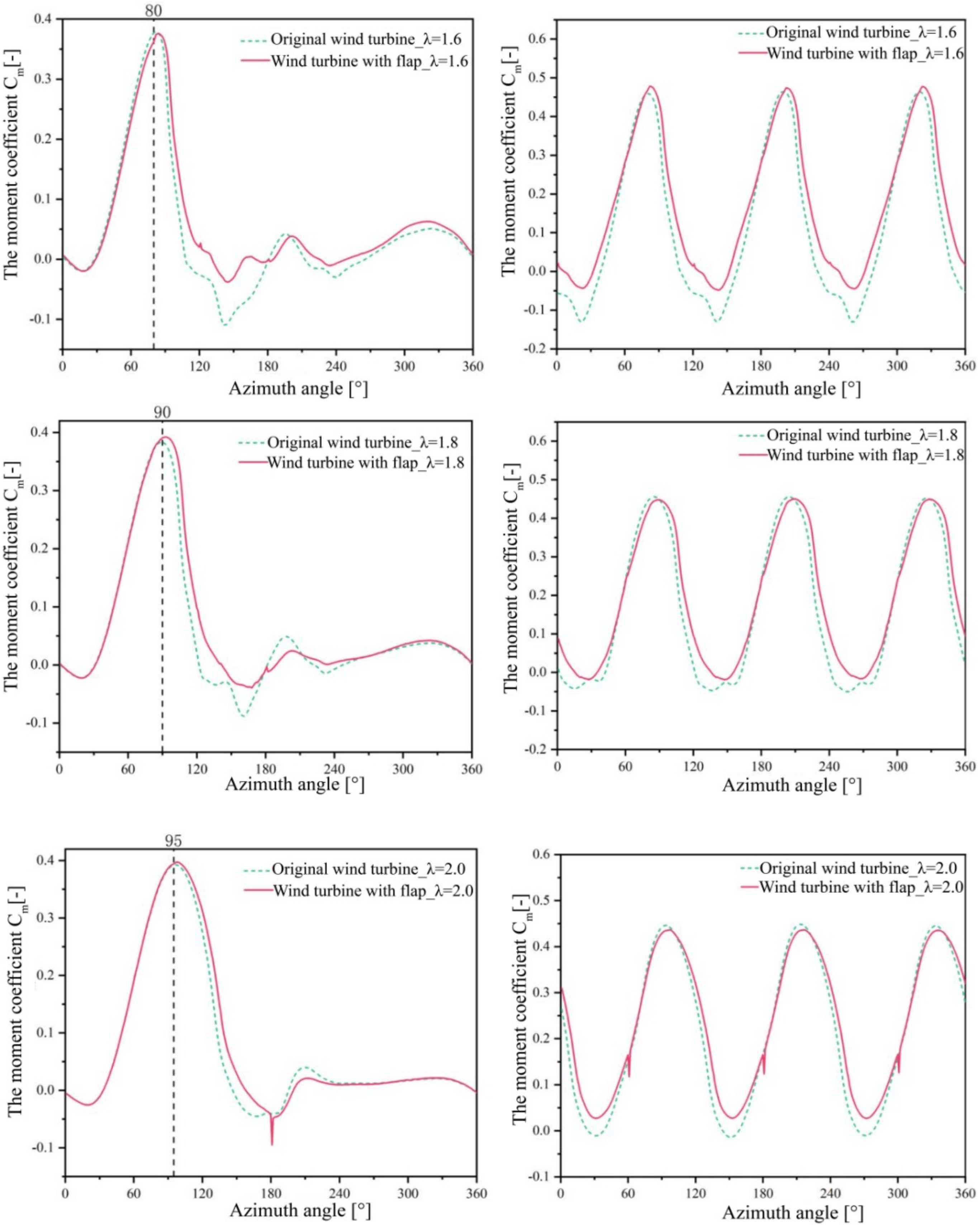

Figure 30. *Variation curve of moment coefficient with azimuth angle for original wind turbine and the wind turbine with the flap.*

Figure 30 shows the variation curves of moment coefficients at different TSRs for the original wind turbine and the wind turbine with flap, the left figures illustrates the single-blade's moment coefficient, while the right figures shows the whole VAWT's moment coefficient. When $\lambda = 1.2$, since the TSR is relatively low and the blades are easy to stall, the single-blade's moment coefficient attains its maximum at an azimuth angle of 68° and then decreases sharply. The single blade's moment coefficient at 68°-180° is higher than that of the original wind turbine. When $\lambda = 1.4$, azimuth ranges from 75° to 180°, the moment coefficient of the single blade of the wind turbine with flap is increased, and its increase is greater than that of $\lambda = 1.2$. In the azimuth range of 180°-360°, the single blade moment coefficient of VAWT with flap becomes flatter.

At right figures, the highest value of moment coefficient for the whole wind turbine of VAWT with flap is lower than the original wind turbine, the lowest value is higher than the original wind turbine, and the fluctuation of moment coefficients are reduced. When $\lambda = 1.6$, the flap has the best effect on moment coefficient, it can be seen that when the azimuth is greater than 80°, the single blade moment coefficient of the VAWT with flap is higher than the original wind turbine except at azimuth angles of about 180°-200°, so the maximum and minimum values of the moment coefficient of the whole wind turbine are improved. When $\lambda = 1.8$ and 2.0, it can be observed that the moment coefficient of the whole wind turbine of the VAWT with flap is only increased at the lowest point and does not change significantly at the highest point. Therefore, the flap can only improve the aerodynamic performance of the VAWT in a specific TSR (when $\lambda = 1.4$ and 1.6), and cannot significantly improve the aerodynamic performance of the VAWT at a higher TSR.

5.1.2. Flow Field Analysis of Flaps on VAWT

In this subsection, the effect of flaps on the flow field in proximity to the wind turbine is analyzed at different TSRs when $\lambda = 1.4$-1.8.

As demonstrated in Figure 31, the size of the vortex near the blades of a wind turbine with flaps is considerably smaller than that of an original wind turbine blade. The flaps delay vortex shedding near the blades, reducing load fluctuations and stabilizing the operation of the VAWT. Consequently, the smaller vortices shed by the flaps have less impact on the downstream blades. As shown above, the flaps are used to control the VAWT at azimuth angles between 80° and 180° when $\lambda = 1.6$.

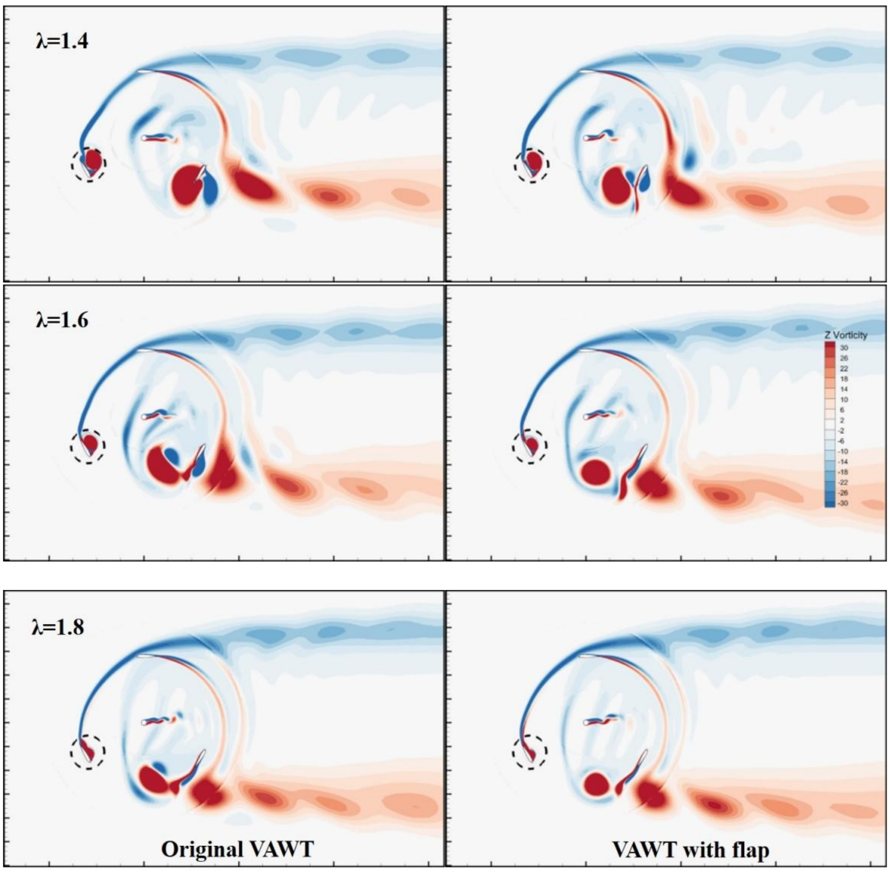

Figure 31. *Vortex wake image of VAWT with flaps at different tip ratios.*

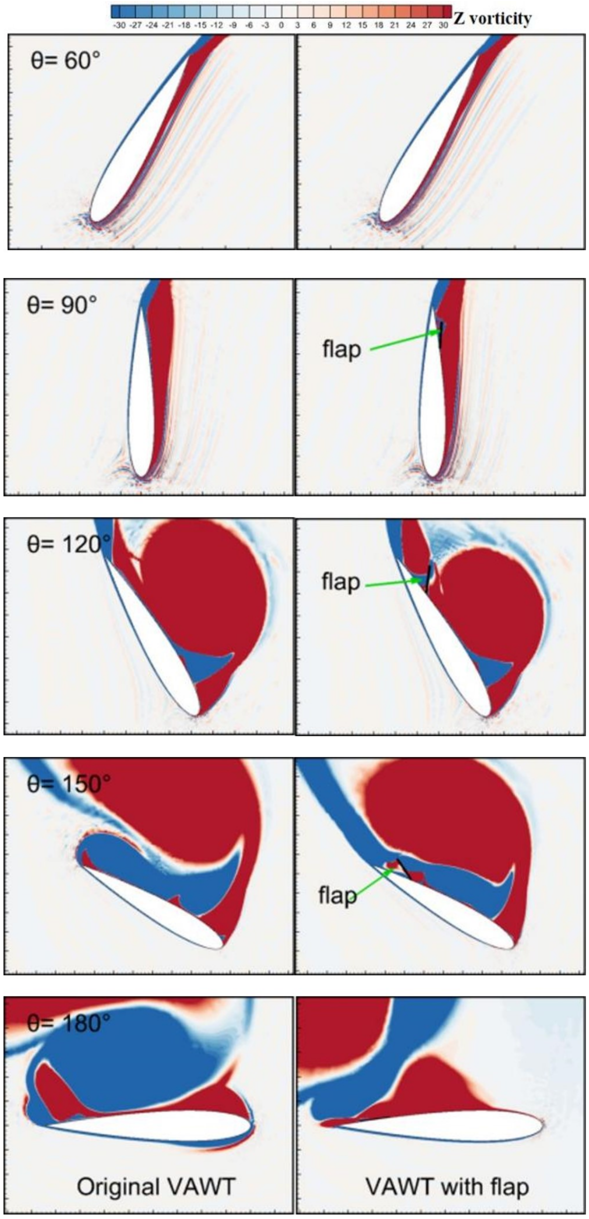

Figure 32. *Vortex image of the original VAWT and the VAWT with flaps when λ = 1.6 in different azimuth.*

Figure 32 shows the vortex image of the original VAWT and the VAWT with flaps at an azimuth angle of θ = 60°-180° and a value of λ = 1.6. When θ = 60°, flow separation only occurs at the trailing edge of the blade due to the small AOA, and the flaps remain closed at this time, so there are no significant changes to the flow fields of the two wind turbines. When θ = 90°, vortex reduction can be seen near the VAWT blades with flaps; however, because the flaps are deployed at a smaller angle, they play a smaller role. At θ = 120°, the flap splits the vortex at the suction surface of the blade, reducing the size of the vortex region. At θ = 150°, the flaps reduce the counter-pressure gradient of the fluid flow near the suction surface of the blade, thereby improving the aerodynamic performance of the VAWT blades. Observation shows that the vortex area above the blades is also significantly reduced. When θ = 180°, the flaps are fully closed, however, the flow near the blades is more stable and the vortex area is smaller due to the effect of the suction surfaces prior to closure.

5.2. Application of Splitter Plate in VAWT

5.2.1. The Effect of the Splitter Plate on the VAWT Aerodynamic Performance

Figure 33 shows the comparison of power coefficient between wind turbine with splitter plate and original wind turbine when the range of λ is 0.4-2.8 and the = 13.45 m/s. It can be seen that the wind turbine with splitter plate exhibits a higher power coefficient than the original wind turbine at different TSRs except when λ is about 1.6.

When λ = 0.4-1.2, power coefficient of wind turbine with splitter plate is higher than the original wind turbine. When l = 0.15c, the value of the increase is 13.43%, 22.27% and

9.53% respectively at the λ of 0.4, 0.8 and 1.2. When l = 0.2c, the value of the increase is 12.35%, 29.39% and 8.41% respectively at the λ of 0.4, 0.8 and 1.2. When λ = 1.6, the power coefficient of the wind turbine with the splitter plate is lower than the original wind turbine. When λ = 2.0, the power coefficient of the wind turbine with splitter plate is almost the same as that of the original wind turbine when l = 0.15c. When l = 0.2c, the power coefficient increased by about 6.29%. The increase in power coefficient at low TSRs indicates that the splitter plate can reduce the effect of dynamic stall at low TSRs and help to improve the self-starting capability of the wind turbine.

At high TSR, the splitter plate can also improve the utilization of wind energy. When l = 0.15c, the value of the increase is 6.21% and 14.21% respectively at the λ of 2.4 and 2.8. When l = 0.2c, the value of the increase is 12.64% and 25.78% respectively at the λ of 2.4 and 2.8. The increase in power coefficient at high TSRs indicates that the splitter plate can extend the range of operating conditions for wind turbines and improve the applicability of the wind turbine. Zamani et al. [22-24] showed that J-shaped airfoils are effective at low TSRs but have limited performance at high TSRs, while Sobhani et al. [20] and Yoo & Oh et al. [21] reported dimple structures that work well in specific TSR intervals. The present splitter plate's performance across a wide TSR range adds to the diverse set of passive flow control solutions for VAWTs. Its simple trailing-edge mounting design also aligns with the practical engineering considerations of Sobhani et al. [20] (avoiding blade stiffness reduction) and Zamani et al. [24] (simplifying structural modification), making it a viable option for VAWT performance optimization.

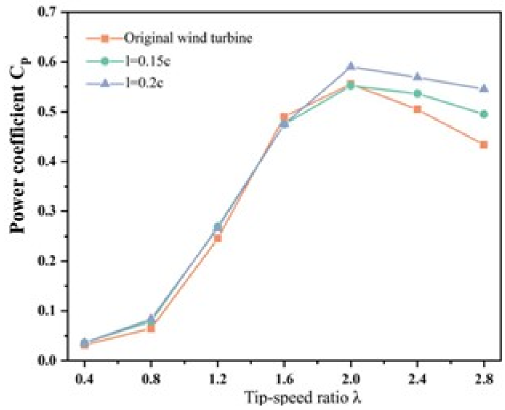

Figure 33. *Comparison of power coefficient between wind turbine with splitter plate and original wind turbine.*

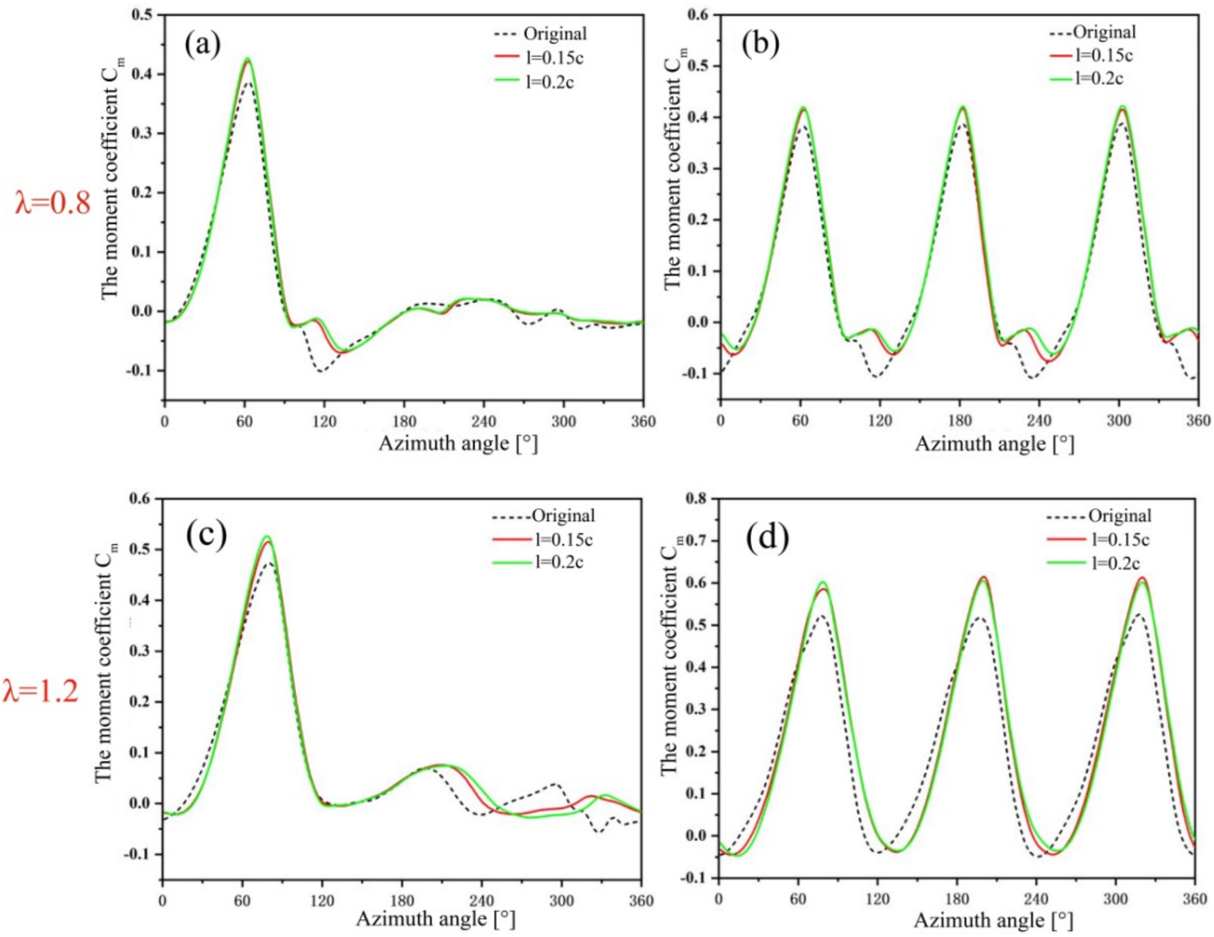

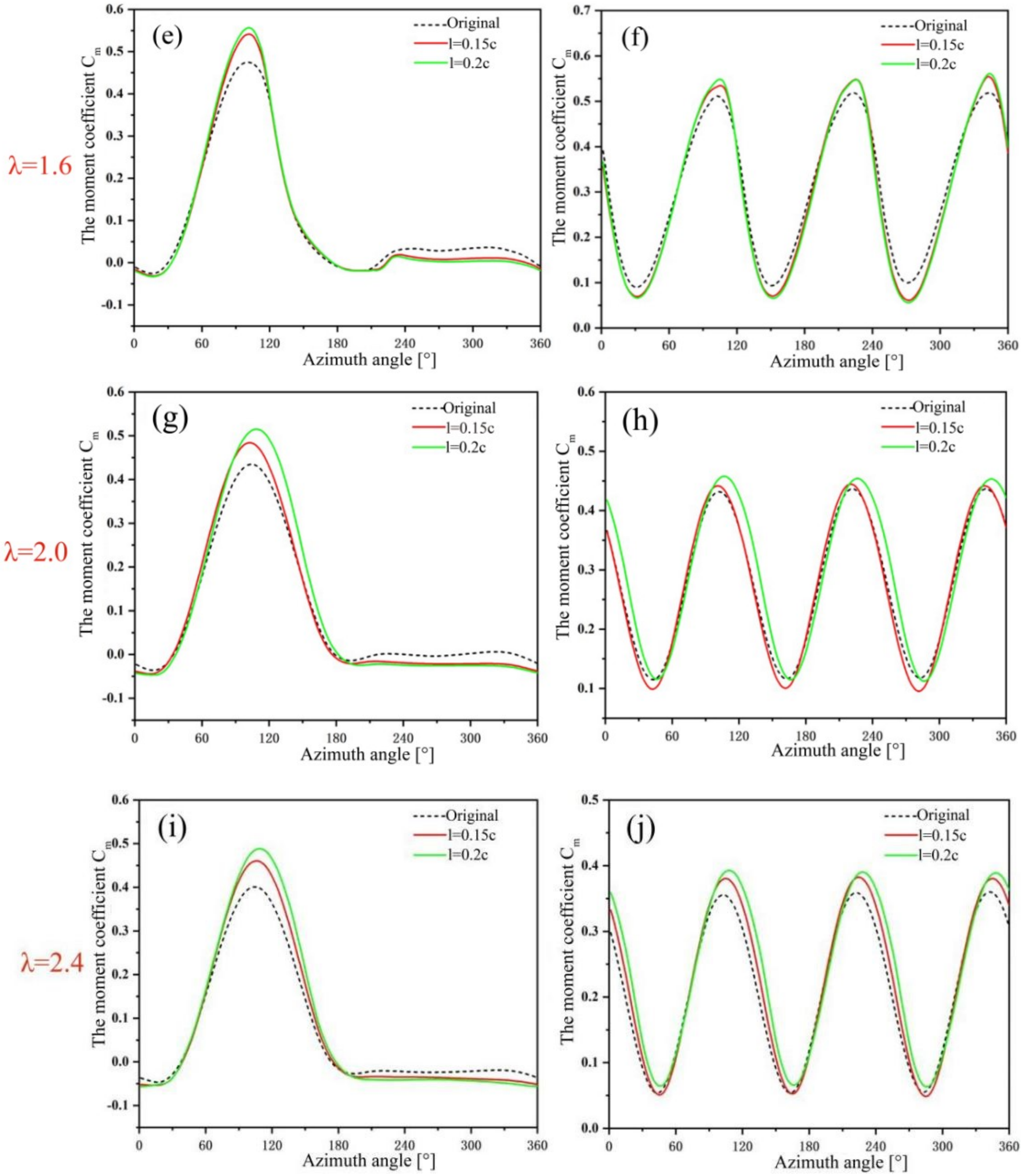

Figure 34. *Variation curve of moment coefficient with azimuth angle for original wind turbine and the wind turbine with the splitter plate.*

Figure 34 shows the curve of moment coefficient varied with azimuth angle for original wind turbine and the wind turbine with the splitter plate. The left figures show the moment coefficient of single blade, the right figures show the moment coefficient of the whole wind turbine.

When $\lambda = 0.8$, since the tip speed is relatively low and the airfoil is prone to dynamic stalls, the moment coefficient of the single blade reaches the maximum value at an azimuthal angle of around 60°. It can be seen that due to the effect of the splitter plate, the moment coefficients of the single blade and the whole wind turbine with the splitter plate are higher those that of the original wind turbine. When $\lambda = 1.2$, for azimuth angles in the range of 60° to 90°, the VAWT single blade moment coefficient with the splitter plate is higher than that of the original wind turbine. It can also be seen from the moment coefficients of the wind turbine as a whole that the maximum and minimum values of the moment coefficients of the VAWT with the splitter plate are higher than those of the original wind turbine.

When λ = 1.6, in the azimuth range from 60° to 140°, the single blade moment coefficient of the wind turbine with a splitter plate is higher than that of the original wind turbine, but the single blade moment coefficient of the wind turbine with a splinter plate is lower than that of the original wind turbine in the azimuth range from 180° to 360°. For the moment coefficient of the whole wind turbine, the maximum value of the moment coefficient of the wind turbine with the splitter plate is higher than that of the original wind turbine, and the minimum value is lower than that of the original wind turbine. When λ = 2.0, the single blade moment coefficient of the wind turbine with splitter plate is higher than that of the original wind turbine when the azimuth range is 60°-180° (windward region) and lower than that of the original wind turbine when the azimuth range is 180°-360° (leeward area). It is worth noting that in the windward region the longer the length of the splitter plate, the greater the increase in the moment coefficient. In the leeward area, the moment coefficients of the two lengths of the splitter plate are almost the same. Hence, the average power coefficient of the whole wind turbine is not much different from that of the original wind turbine when l = 0.15c, but the power coefficient is greatly improved when l = 0.2c.

5.2.2. Analysis of Wind Turbine Flow Field Characteristics

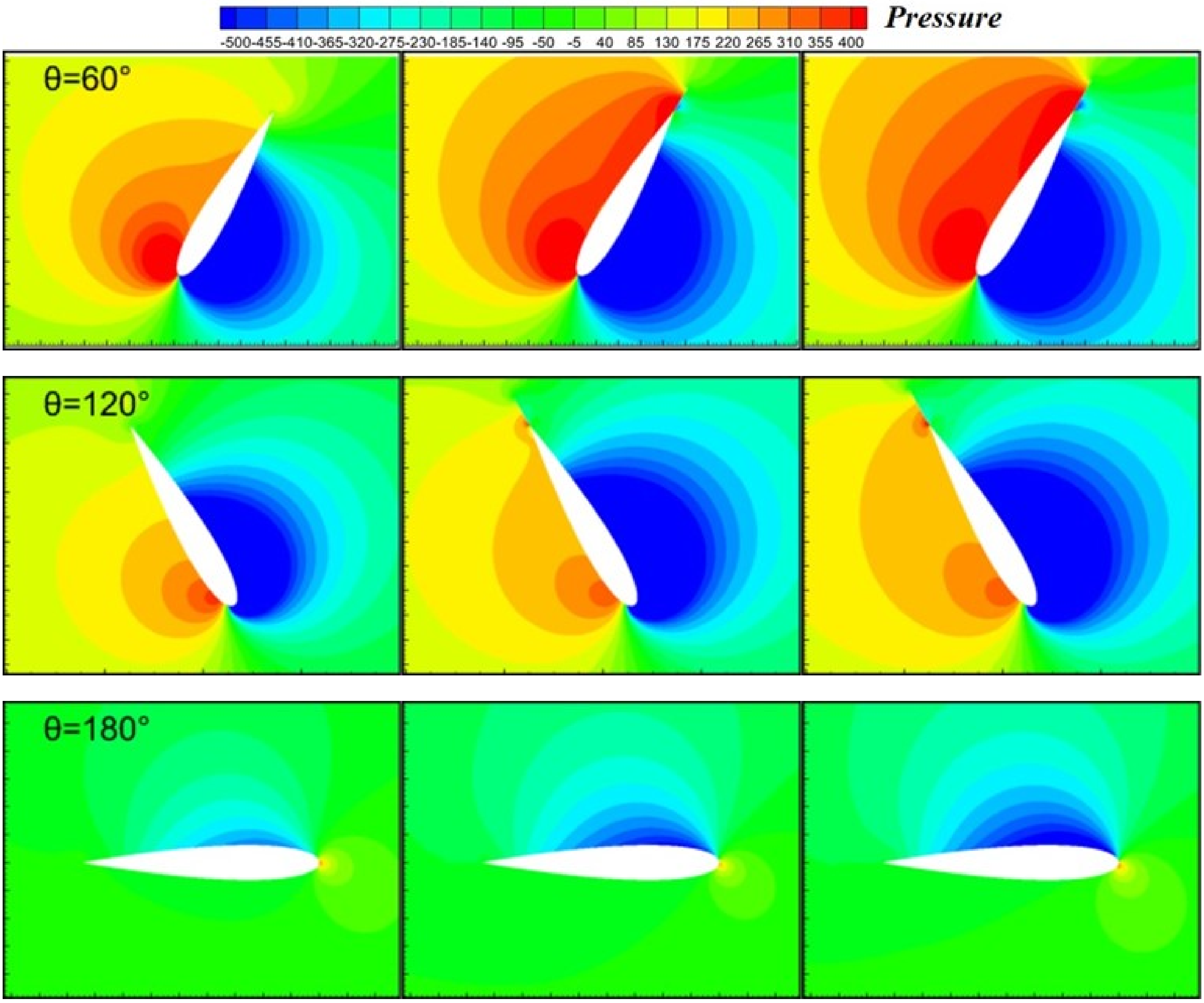

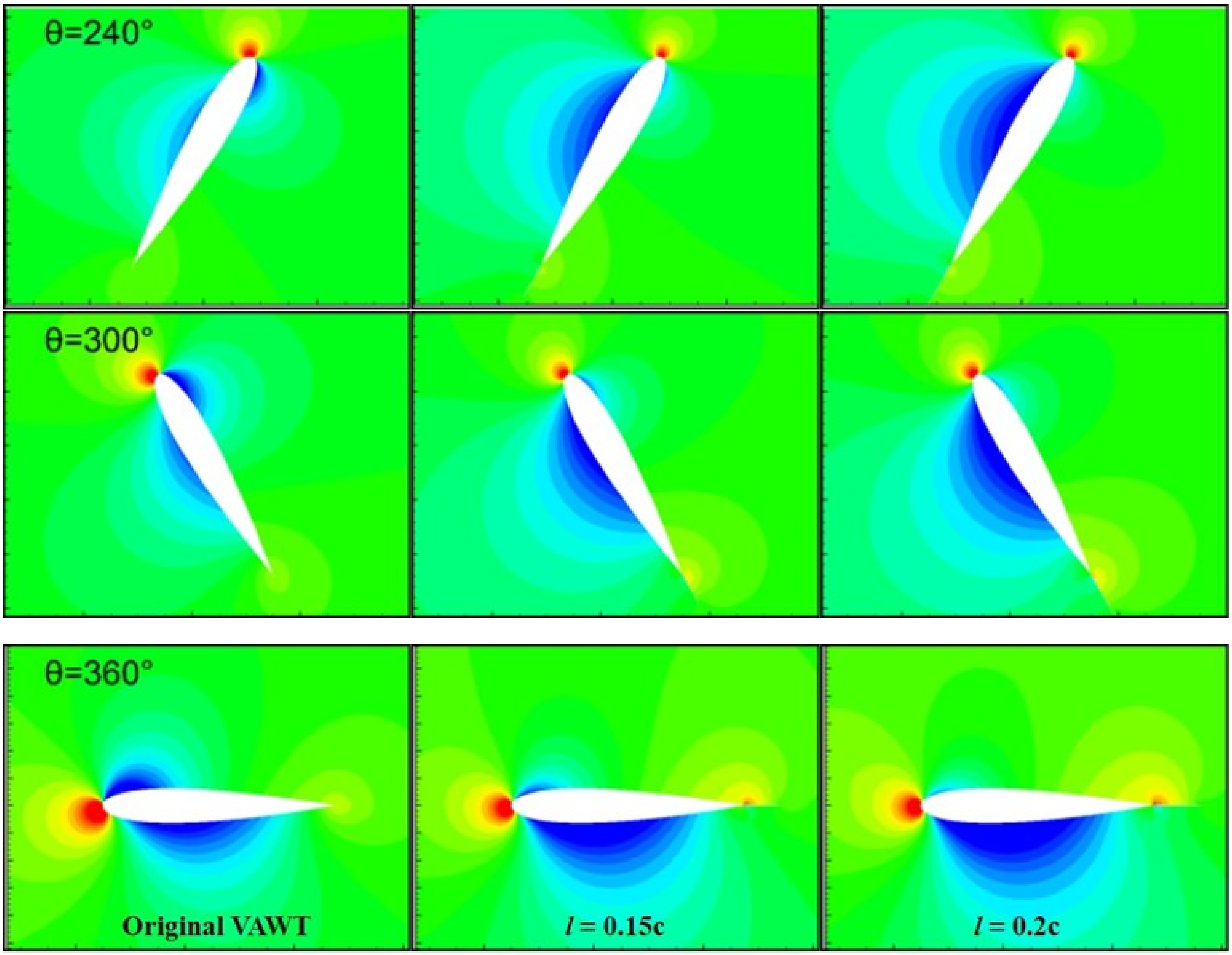

Figure 35. *Pressure image near the blades of VAWT at different azimuth angles for λ = 1.6.*

Figure 35 shows the pressure contours near the blades of a VAWT at different azimuth angles for λ = 2.4. For θ = 60°, a large positive pressure is present on the forward part of the pressure surface of the original wind turbine blades, and a large negative pressure is present on the suction surface of the blades. This creates a pressure difference between the two sides of the blade, resulting in a tangential force acting on the blade. For the splitter plate, the positive pressure values on the blade's pressure surface increase significantly and the range of regions with large positive pressure values expands. The longer the splitter plate, the more useful it is in helping the blade to obtain greater tangential force. When θ = 120°, the maximum pressure value at the leading edge of the pressure surface of the blade with the splitter plate is smaller than that of the original VAWT blade. However, the positive pressure range of the pressure surface increases and the negative pressure range of the suction surface is larger. When θ = 180°, the negative pressure region inside the blade increases for the splitter plate, but this has less impact as the blade is parallel to the direction of the incoming flow and has less ability to do work. When θ = 240° and 300°, the splitter plate begins to have a negative impact. Due to the effect of the splitter plate, the positive pressure at the leading edge of the blade is reduced and a larger area of negative pressure is produced on the blade's pressure surface. This causes the wind turbine to produce a larger torque force in the opposite direction to the rotation. At θ = 360°, a larger area of negative pressure is produced on the outside of the blades, similar to at θ = 180°, when the blades are parallel to the direction of the incoming flow, so the splitter plate has a smaller negative effect.

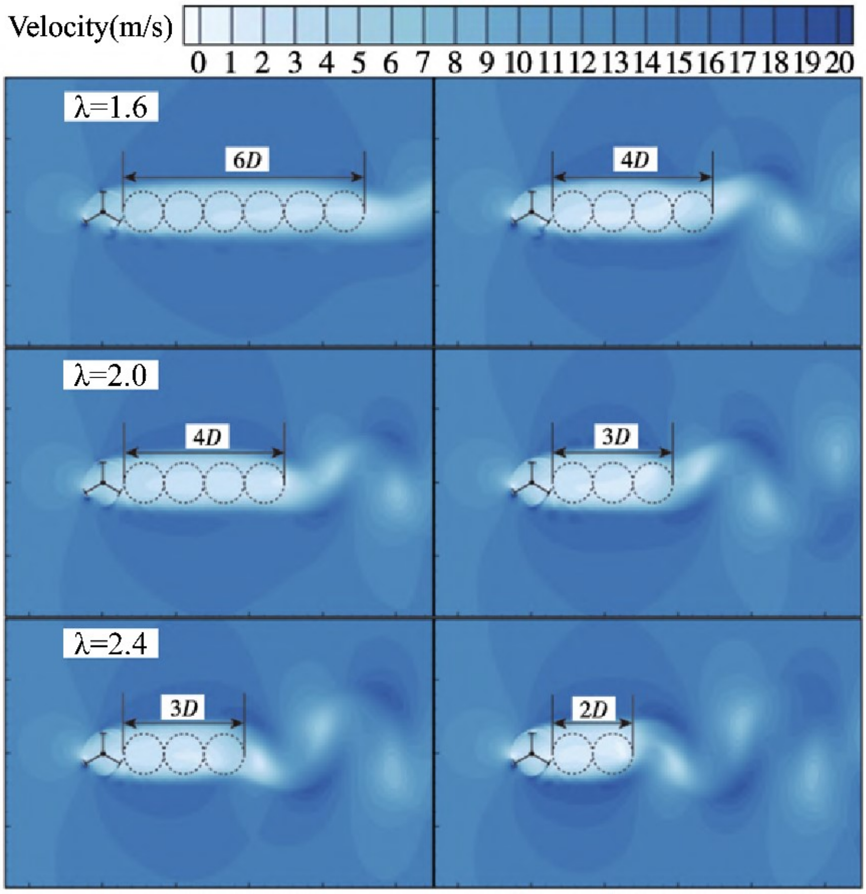

Figure 36. *Velocity image of wake streams of two wind turbines with different TSRs*

Figure 36 shows the velocity image of the wake of two wind turbines with different TSRs. It can be seen that, as the TSR increases, the wake length of the wind turbine decreases and the wake flow recovers faster. At the same TSR, the wake length of the wind turbine with the splitter plate is shorter than that of the original wind turbine. Clearly, the splitter plate plays a pivotal role in recovering the wake flow of wind turbines, thereby enhancing the downstream turbines' aerodynamic performance. This, in turn, reduce the installation distance between wind turbines and improve the power density per unit area.

6. Conclusion

In this paper, the aerodynamic performance of the airfoil with the plate and splitter plate in different AOA were investigated and the plate and splitter plate are applied to VAWT and their effects on the aerodynamic performance of VAWT are investigated. The main results observed in this study are summarized as followed:

(1) The conclusion for the airfoil:

1) For flap on suction surface: After stall AOA, the flaps impede the inverse pressure gradient flow from the trailing edge to the leading edge at the suction surface of the airfoil, and improving its aerodynamic performance. And flaps are better placed on the airfoil near the trailing edge, but not as close to the trailing edge as possible. Flaps at different AOA have an optimal deployment angle, and the optimal deployment angle increases with the AOA, but not linearly.

2) For splitter plate: Before stall AOA, the splitter plate can have the effect of increasing lift and reducing drag, and the longer the length of the splitter plate, the better the LDR enhancement, with a maximum increase in LDR of about 61.6% (l = 0.2c). The positive effect of the splitter plate on the airfoil decreases as f increases, with the best results at f = 0.01c. And in the full stall phase, the splitter plate can also improve the LDR of the airfoil, but the optimal f varies at different AOA.

(2) The conclusion for VAWT:

1) The flaps can significantly reduce the vortex size near the blades and promote vortex shedding near the blades. At λ = 1.2˜2.0, the flaps can improve the power coefficient factor of the VAWT by up to 42.5% (λ = 1.6).

2) The splitter plate can increase the power coefficient of the VAWT by a maximum of about 29.4% (λ = 0.8) at low TSRs (λ = 0.4 to 1.2). At high TSRs (λ = 2.0 to 2.4), the splitter plate can increase the power coefficient by a maximum of about 25.8% (λ = 2.8).

Abbreviations

AOA	Angle of Attack
CFD	Computational Fluid Dynamics
C_D	Drag Coefficient
C_L	Lift Coefficient
C_m	Moment Coefficient
C_p	Power Coefficient
DNS	Direct Numerical Simulation
HAWT	Horizontal Axis Wind Turbine
k-ε	k-Epsilon Turbulence Model
k-ω	k-Omega Turbulence Model
LDR	Lift-Drag Ratio
LES	Large Eddy Simulation
NACA	National Advisory Committee for Aeronautics
PIV	Particle Image Velocimetry
RANS	Reynolds-Averaged Navier-Stokes
Re	Reynolds Number
S-A	Spalart-Allmaras Turbulence Model
SST	Shear Stress Transport (Turbulence Model)
TSR	Tip Speed Ratio
UDF	User-Defined Function
VAWT	Vertical Axis Wind Turbine
y$^+$	y-Plus (Wall Distance Parameter)

Acknowledgments

The authors express their great thanks to National Key R&D Program of China. Project Number: 2024YFA1012501 for financial support. This work is also supported by National Natural Science Foundation of China with Grant No.52276031.

Data Availability

The data that support the findings of this study are available from the corresponding author upon reasonable request.

Conflicts of Interest

The authors declare no conflicts of interest.

References

[1] Wang J Z, Feng G F, Yin H T, et al. Toward sustainable development: Does the rising oil price stimulate innovation in climate change mitigation technologies [J]. Economic Analysis and Policy, 2023, 79: 569-583. https://doi.org/10.1016/J.EAP.2023.06.034

[2] Koh J H, Ng E Y K. Downwind offshore wind turbines: Opportunities, trends and technical challenges[J]. Renewable and Sustainable Energy Reviews, 2016, 54: 797-808. https://doi.org/10.1016/j.rser.2015.10.096

[3] Mudgal T, Tiwari M, Bharti D. Cylindrical-electrode triboelectric nanogenerator for low-speed wind energy harvesting[J]. Nano Energy, 2024, 123: 109388. https://doi.org/10.1016/J.NANOEN.2024.109388

[4] Jiang Y, Chen P, Wang S, et al. Dynamic responses of a 5 MW semi-submersible floating vertical-axis wind turbine: A model test study in the wave basin [J]. Ocean Engineering, 2024, 296: 117000. https://doi.org/10.1016/J.OCEANENG.2024.117000

[5] Ahmad H, Amne E, Michel E. Numerical investigation of the use of flexible blades for vertical axis wind turbines [J]. Energy Conversion and Management, 2024, 299: 117867. https://doi.org/10.1016/J.ENCONMAN.2023.117867

[6] Tummala A, Velamati K R, Sinha K D, et al. A review on small scale wind turbines [J]. Renewable and Sustainable Energy Reviews, 2016, 56: 1351-1371.

[7] Peng H Y, Liu H J, Yang J H. A review on the wake aerodynamics of H-rotor vertical axis wind turbines [J]. Energy, 2021, 232: 121003. https://doi.org/10.1016/J.ENERGY.2021.121003

[8] L. N. A. Vertical axis wind turbines in cluster configurations [J]. Ocean Engineering, 2023, 272: 113855. https://doi.org/10.1016/J.OCEANENG.2023.113855

[9] Trauernicht N, Miguda H, Martinetti A. Design guidelines for HAWT / VAWT decision-making in the context of underserved communities [J]. Procedia CIRP, 2024, 128: 448-453. https://doi.org/10.1016/J.PROCIR.2024.03.025

[10] Ahmed A, Hani G, Gamal E, et al. A novel VAWT passive flow control numerical and experimental investigations: Guided Vane Airfoil Wind Turbine [J]. Ocean Engineering, 2022, 257: 111704. https://doi.org/10.1016/J.OCEANENG.2022.111704

[11] Ashill P. Flow Control: Passive, Active, and Reactive Flow Management [J]. The Aeronautical Journal (1968), 2001, 105 (1045): 150-150. https://doi.org/10.1017/S000192400009206X

[12] Yaoru Q, Yuquan Z, Yukun S, et al. Numerical investigations of the flow control effect on a thick wind turbine airfoil using deformable trailing edge flaps [J]. Energy, 2023, 265: 126327. https://doi.org/10.1016/J.ENERGY.2022.126327

[13] Carla A, Amne E, Joelle N, et al. Performance enhancement of a vertical axis wind turbine using a slotted deflective flap at the trailing edge [J]. Energy Conversion and Management, 2022, 273: 116388. https://doi.org/10.1016/J.ENCONMAN.2022.116388

[14] Peilin W, Qingsong L, Chun L, et al. Investigation of the aerodynamic characteristics of horizontal axis wind turbine using an active flow control method via boundary layer suction [J]. Renewable Energy, 2022, 198: 1032-1048. https://doi.org/10.1016/J.RENENE.2022.08.075

[15] Sun Y, Qian Y, Wang T, et al. Investigation of the wind turbine aerodynamic performance via the combining blowing and suction flow control [J]. Energy, 2024, 307: 132505. https://doi.org/10.1016/J.ENERGY.2024.132505

[16] Aram E, Mittal R, Cattafesta L. Simple Representations of Zero-Net Mass-Flux Jets in Grazing Flow for Flow-Control Simulations [J]. International Journal of Flow Control, 2010, 2 (2): 109-125. https://doi.org/10.1260/1756-8250.2.2.109

[17] Zhu H, Guo H, Sun J, et al. Research Progress on Active Secondary Jet Technology in Supersonic Flow Field of Aerospace Propulsion Systems [J]. Fluids, 2023, 8 (12): 313. https://doi.org/10.3390/FLUIDS8120313

[18] Liu Q, Miao W, Li C, et al. Effects of trailing-edge movable flap on aerodynamic performance and noise characteristics of VAWT [J]. Energy, 2019, 189: 116271. https://doi.org/10.1016/j.energy.2019.116271

[19] Satar A H M, Razak N, Abdullah S M, et al. A comprehensive comparison of passive flow controls on the wind turbine blade lift and drag performances: A CFD approach [J]. European Journal of Mechanics / B Fluids, 2024, 108: 119-133. https://doi.org/10.1016/J.EUROMECHFLU.2024.07.009

[20] Sobhani E, Ghaffari M, Maghrebi J M. Numerical investigation of dimple effects on darrieus vertical axis wind turbine [J]. Energy, 2017, 133: 231-241. https://doi.org/10.1016/j.energy.2017.05.105

[21] Seungwoo Y, Sahuck O. Flow analysis and optimization of a vertical axis wind turbine blade with a dimple [J]. Engineering Applications of Computational Fluid Mechanics, 2021, 15 (1): 1666-1681. https://doi.org/10.1080/19942060.2021.1989041

[22] Zamani M, Nazari S, Moshizi A S, et al. Three dimensional simulation of J-shaped Darrieus vertical axis wind turbine [J]. Energy, 2016, 116: 1243-1255. https://doi.org/10.1016/j.energy.2016.10.031

[23] Mohamed M. Criticism study of J-Shaped darrieus wind turbine: Performance evaluation and noise generation assessment [J]. Energy, 2019, 177: 367-385. https://doi.org/10.1016/j.energy.2019.04.102

[24] Zamani M, Maghrebi J M, Moshizi A S. Numerical study of airfoil thickness effects on the performance of J-shaped straight blade vertical axis wind turbine [J]. Wind and Structures, 2016, 22 (5): 595-616. https://doi.org/10.12989/WAS.2016.22.5.595

[25] Shukla V, Kaviti K A. Performance evaluation of profile modifications on straight-bladed vertical axis wind turbine by energy and Spalart Allmaras models [J]. Energy, 2017, 126: 766-795. https://doi.org/10.1016/j.energy.2017.03.071

[26] Luo D, Huang D, Sun X. Passive flow control of a stalled airfoil using a microcylinder [J]. Journal of Wind Engineering & Industrial Aerodynamics, 2017, 170: 256-273. https://doi.org/10.1016/j.jweia.2017.08.020

[27] Bramesfeld G, Maughmer D M. Experimental Investigation of Self-Actuating, Upper-Surface, High-Lift-Enhancing Effectors [J]. Journal of aircraft, 2002, 39 (1): 120-124.

[28] Brücker C, Weidner C. Influence of self-adaptive hairy flaps on the stall delay of an airfoil in ramp-up motion [J]. Journal of Fluids and Structures, 2014, 47: 31-40. https://doi.org/10.1016/j.jfluidstructs.2014.02.014

[29] Zikang Z, Shengxian H, Ying W. Numerical simulation study of the fluid-structure coupling effects of Kármán vortex street on airfoil motion with varying thickness [J]. Ocean Engineering, 2023, 286 (P2): 115459. https://doi.org/10.1016/J.OCEANENG.2023.115459

[30] Zhou J, Qiu X, Li J, et al. The experimental investigation on wake dynamics of flow around a circular cylinder with the splitter plate [J]. Journal of Fluids and Structures, 2024, 127: 104130. https://doi.org/10.1016/J.JFLUIDSTRUCTS.2024.104130

[31] Shen P, Zhao W, Zhang H, et al. Force and vortex shedding characteristics of a circular cylinder with flexible splitter plates [J]. Experimental Thermal and Fluid Science, 2024, 154: 111150. https://doi.org/10.1016/J.EXPTHERMFLUSCI.2024.111150

[32] Eike T, Markus K. On hybrid RANS-LES of transition in a separated boundary layer [J]. International Journal of Heat and Fluid Flow, 2023, 103: 109188. https://doi.org/10.1016/J.IJHEATFLUIDFLOW.2023.109188

[33] K. R K, M. P G. Effect of best position blade pitching on power coefficient of VAWT at different tip speed ratio by SST & DMST model [J]. FME Transactions, 2018, 46 (4): 560-566. https://doi.org/10.5937/fmet1804560k